Radiology

Diffusion-weighted MR Imaging of the Liver[1]

Bachir Taouli, MD
Dow-Mu Koh, MD, MRCP, FRCR

Magnetic resonance (MR) imaging plays an increasingly important role in the evaluation of patients with liver disease because of its high contrast resolution, lack of ionizing radiation, and the possibility of performing functional imaging sequences. With advances in hardware and coil systems, diffusion-weighted (DW) MR imaging can now be applied to liver imaging with improved image quality. DW MR imaging enables qualitative and quantitative assessment of tissue diffusivity (apparent diffusion coefficient) without the use of gadolinium chelates, which makes it a highly attractive technique, particularly in patients with severe renal dysfunction at risk for nephrogenic systemic fibrosis. In this review, acquisition parameters, postprocessing, and quantification methods applied to liver DW MR imaging will be discussed. The current clinical uses of DW MR imaging (liver lesion detection and characterization, compared and combined with conventional sequences) and the emerging applications of DW MR imaging (tumor treatment response and diagnosis of liver fibrosis and cirrhosis) will be reviewed. Also, limitations, mainly image quality and reproducibility of diffusion parameters, and future directions of liver DW MR imaging will be discussed.

© RSNA, 2010

Radiology

Since the first brain diffusion imaging in 1986 (1) and the widespread application for stroke detection in the early 1990s (2–6), diffusion-weighted (DW) magnetic resonance (MR) imaging has evolved into a mature functional MR imaging technique for many brain imaging applications (7,8). With recent advances in technology, DW MR imaging is reaching a potential for clinical use in the abdomen, particularly in the liver. DW MR imaging is an attractive technique for multiple reasons: it can potentially add useful qualitative and quantitative information to conventional imaging sequences; it is quick (performed within a breath hold) and can be easily incorporated to existing protocols; and it is a nonenhanced technique (performed without the use of gadolinium-based contrast media), thus easy to repeat, and useful in patients with severe renal dysfunction at risk for nephrogenic systemic fibrosis (9–12). However, liver DW MR imaging is still in its infancy and is faced with many challenges before being fully validated for liver imaging applications.

In this review, we will discuss the acquisition, postprocessing, quantification methods, and results of DW MR imaging applied for the diagnosis of diffuse and focal liver diseases.

Essentials

- Diffusion-weighted (DW) MR imaging can be used for liver lesion detection and characterization, with better results compared with T2-weighted imaging and with potential additional value to contrast-enhanced sequences.

- Emerging promising applications of DW MR imaging include assessment of treatment response and detection of liver fibrosis and cirrhosis, requiring further confirmation.

- In patients who cannot receive gadolinium-based contrast agents, DW MR imaging has the potential to be a reasonable alternative technique to contrast-enhanced imaging.

Principles of Diffusion-weighted Imaging in the Liver

Diffusion is a physical process that results from the thermally driven, random motion of water molecules (13,14). In a container of water, molecules undergo free, thermally agitated diffusion (with a three-dimensional Gaussian distribution). The width of the Gaussian distribution expands with the elapsed time, and the average square of this width per unit time gives the units of the apparent diffusion coefficient (ADC) (see below). In tissues, apparent diffusion is observed since the movement of water molecules is modified by their interactions with cell membranes and macromolecules. DW MR imaging is an MR imaging technique that derives its image contrast on the basis of differences in the mobility of protons (primarily associated with water) between tissues. In tissues that are highly cellular (eg, tumor tissues), the tortuosity of the extracellular space and the higher density of hydrophobic cellular membranes restrict the apparent diffusion of water protons (15,16). In such an environment, water diffusion is said to be relatively "restricted." By contrast, in cystic or necrotic tissues, the apparent diffusion of water protons is relatively "free." Thus, DW MR imaging is unique in its ability to provide information that reflects tissue cellularity and the integrity of cellular membranes (17).

Stejskal and Tanner (18) were the first to describe an MR experiment that could be used to observe and measure water diffusion. They modified a standard T2-weighted imaging sequence by applying a symmetric pair of diffusion-sensitizing gradients on either side of the 180° refocusing pulse (Fig 1). Moving water protons acquire a phase shift from the first diffusion-sensitizing gradient, which, as a consequence of motion, is not entirely rephased by the second gradient, resulting in attenuation of the measured signal intensity. Hence, the presence of water diffusion is observed as signal loss on DW MR images. As stated previously, the phenomenon of diffusion resembles a three-dimensional distribution; however, in a

single diffusion-encoded image (such as done with the pulse sequence in Fig 1), diffusion only along the direction of the diffusion-encoding gradients is measured. Liver DW MR imaging is routinely estimated by using tridirectional diffusion gradients along each of the three directions (x, y, and z), and the average diffusion-weighted image (trace) is evaluated. However, water motion can occur preferentially in some directions in certain tissues (anisotropic tissues) due to presence of obstacles that limit molecular movement in some directions. Diffusion anisotropy can be detected by observing differences in diffusivity in different diffusion directions, such as in brain white matter (19–21), spinal cord (22), muscle (23), and renal medulla (24,25). By using diffusion gradients in at least six directions, diffusion-tensor imaging can be used to obtain anisotropy information (fractional anisotropy and other indexes) (8), in addition to ADC. Diffusion-tensor imaging has been used predominantly for brain imaging (8,14,21,26–30), with limited data for body imaging of liver (31,32), kidneys (24,25), or prostate (33,34). A prior study showed minimal nonsignificant differences in ADC values between the three diffusion-gradient directions (35), proving the isotropic structure of liver parenchyma. Two other studies reported use of liver diffusion-tensor imaging in association with parallel imaging (31,32). However, none of these studies have described specifically fractional anisotropy values in the liver. In our experience, we found fractional anisotropy maps of the liver to be noisy (due to short liver T2) and

Figure 1

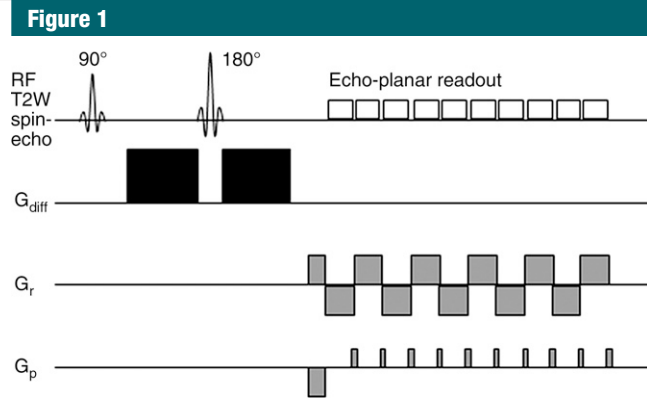**Figure 1:** Gradient acquisition scheme according to a Stejskal-Tanner SE echo-planar DW MR imaging experiment. Note the diffusion-sensitizing gradients (in black), which are placed on either side of the 180° refocusing pulse, and the echo-planar readout, which results in rapid image acquisition. *RF* = radiofrequency.

therefore not diagnostic, at least using the current technology.

The sensitivity of the imaging sequence to water diffusion can be altered by changing the *b* value, or *b* factor, which is dependent in a specific mathematical way on the diffusion-encoding gradient waveforms (13). The *b* value increases with the square of the gradient amplitude, the square of the gradient diffusion length, and approximately with the time between the two pulses, as shown in the following equation: *b* (in in seconds per square millimeter) $= \gamma^2 \, G^2 \, \delta^2 \, (\Delta - \delta/3)$, where γ is the gyromagnetic ratio, G is the diffusion gradient amplitude, δ is the gradient diffusion length, and Δ is the diffusion time.

The signal intensity from protons with larger diffusion distances per unit time (eg, blood flow) is attenuated with small *b* values (eg, *b* < 100–150 sec/mm^2). By comparison, when higher *b* values (eg, > 500 sec/mm^2) are used, there is usually less signal attenuation from cellular tumors containing protons with shorter diffusion distances, compared with the normal liver. Thus, performing DW MR imaging measurements by using two or more *b* values, tumor detection and characterization are possible based on the differences in water diffusivity. The images from each individual *b* value can be assessed qualitatively. However, performing imaging by using two or more *b* values also allows quantification of the ADC of tissues. The

process of ADC calculation is usually automated with clinical MR systems. In mathematical terms, this is achieved for each voxel on the diffusion image by performing a monoexponential fit to the relationship between the measured signal intensity (in logarithmic scale) and the *b* values as follows: ADC = ln (SI$_0$/SI)/ *b*, where SI$_0$ is signal intensity for *b* = 0 and SI is that for a higher *b* value.

The slope of the line that describes this relationship in each voxel represents the ADC (Fig 2). The calculated ADC values for all voxels are usually displayed as a parametric map, and by drawing a region of interest onto this map, the mean or median ADC value in the region of interest that reflects water diffusivity can be recorded. ADC measurements in the liver have been used for tumor detection and characterization, as well as for assessment of tumor response to treatment and diagnosis of fibrosis and cirrhosis.

Interestingly, it has been shown that the degree of signal attenuation of the liver and focal liver lesions with increasing *b* value is nonlinear, due to microcapillary perfusion (36–39). A biexponential behavior has been observed over the range of *b* values used for clinical imaging, where initially a small increase in *b* value (in the range of 0–200 sec/mm^2) results in a steep reduction in the measured signal intensity (Fig 2). The signal then attenuates more gradually over the range of higher *b* values ($\geq$ 200 sec/mm^2). This is explained by the in-

travoxel incoherent motion, or IVIM, phenomenon, or pseudo-diffusion effect, in relation to capillary perfusion (36,39–42). With IVIM, molecular diffusion can be separated from perfusion, provided that a wide range of *b* values (including low [< 200 sec/mm^2] and high [$\geq$ 200 sec/mm^2]) are used (36). Understanding this phenomenon is important because the choice of *b* values can determine the degree to which the calculated ADC may be influenced by tissue perfusion at low *b* values, as this may confound the measurement of tissue diffusivity. This explains why ADCs of liver lesions reported in the literature calculated by using only lower *b* values (< 100–200 sec/mm^2) (38,39,43,44) are higher than those obtained by using higher or a wider range of *b* values (35,45,46). By contrast, ADCs calculated by using only higher *b* values ($\geq$ 200 sec/mm^2) (47) or with a more sophisticated data fitting using the principles of IVIM (39) are lower than those calculated by using a wide range of *b* values (which includes lower *b* values), because the perfusion effects are excluded.

Liver Diffusion Imaging Acquisition, Optimization, and Display

DW MR Imaging Acquisition Techniques

Although a number of imaging sequences can be applied to evaluate the liver, single-shot spin-echo (SE) echo-planar technique is the most frequently used in combination with fat suppression (eg, spectral attenuated inversion recovery or chemical excitation with spectral suppression) (20,48–50) (Fig 1). Because single-shot SE echo-planar sequences are intrinsically sensitized to the motion of diffusion, they are generally also highly sensitive to other kinds of motion, such as bulk motion and respiration, which may produce artifacts. Thus, diffusion acquisitions are generally designed to attempt to avoid or account for these latter effects. Most DW MR imaging studies have been conducted by using 1.5-T MR systems, although there is a growing interest in performing such studies with 3.0-T systems due to increased availability and potential for improved image quality (51,52).
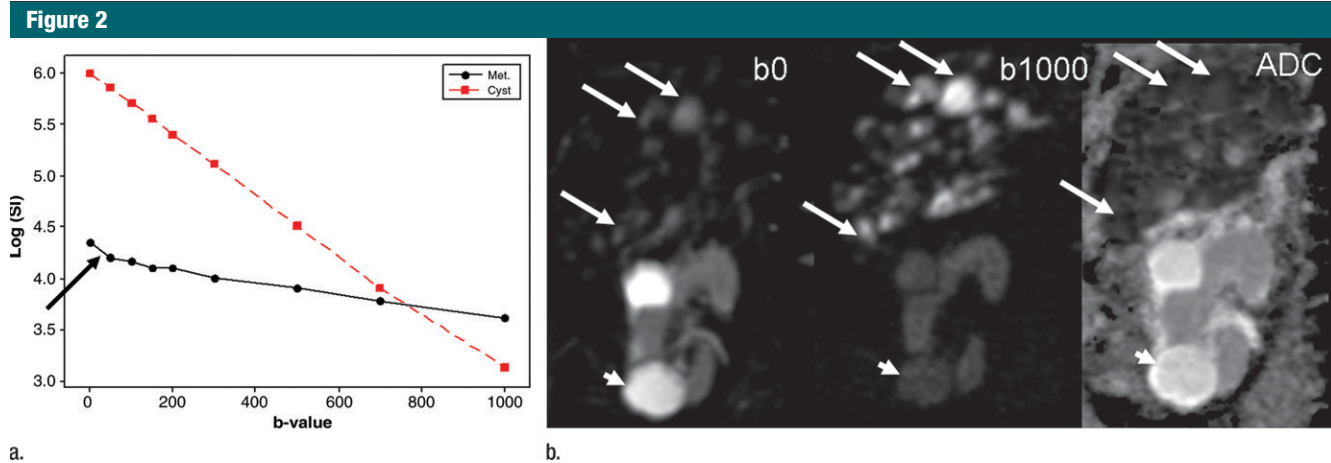
Figure 2: ADC calculation and intravoxel incoherent motion (IVIM) MR effect in a 78-year-old man with liver metastases from lung cancer and renal cysts. **(a)** The ADC is calculated over the entire range of b values used at imaging as a simple monoexponential fit of log signal intensity *(SI)* versus b values: $S = S_0 \times \exp(-b \times \text{ADC})$, where S is the signal intensity after application of the diffusion gradient and S_0 is the signal intensity at b of 0 sec/mm^2 (the ADC represents the slope of the curve). **(b)** Fits of benign renal cyst (short arrows) and liver metastases (long arrows) are represented on top and corresponding coronal single-shot SE echo-planar images ($b = 0$–1000 sec/mm^2) and ADC maps are represented on the bottom. The cyst demonstrates strong straight signal attenuation, whereas the metastatic lesion has minimal signal decrease, consistent with restricted diffusion, with an initial strong signal decrease related to IVIM effect (arrow on **a**). ADC (x 10^{-3} mm^2/sec, using all b values) was 2.8 and 0.70 for the cyst and the metastasis, respectively.

DW MR imaging of the liver is usually performed prior to contrast material administration, although performing DW MR imaging after the administration of gadopentetate dimeglumine did not appear to significantly affect ADC calculations in a prior study (53). Imaging may be performed during a breath hold, which attempts to freeze motion, or during free breathing with multiple signal acquisitions to reduce the effects of motion. Image acquisition during free breathing may also be combined with respiratory (54) and/or cardiac triggering (55). Breath-hold single-shot SE echo-planar imaging of the liver is quick to perform, and the whole liver can be evaluated in generally one or two breath holds of 20–30 seconds each, depending on liver size and sequence parameters. However, the disadvantages of breath-hold imaging include poorer signal-to-noise ratio (SNR), greater sensitivity to distortion and ghosting artifacts, lower spatial resolution (with wider section thickness, 8–10 mm), and a limitation on the number of b values that can be included in the measurement.

By comparison, free-breathing multiple-signal-acquisition single-shot SE echo-planar imaging is a versatile technique that can be implemented rea-sonably well across different vendor MR platforms. The liver is typically evaluated in 3–6 minutes. The use of multiple signal acquisitions results in images with improved SNR. Consequently, thinner image sections ($\geq$ 5 mm) can be obtained, and more b values can be accommodated within the longer measurement. High-quality diffusion images of the liver can be obtained by using a free-breathing technique because cyclical respiration is a coherent motion that does not result in additional signal attenuation from the liver (56). The disadvantages include slight image blurring and assessment of lesion heterogeneity that may be suboptimal because of volume averaging. Free-breathing DW MR imaging may be combined with respiratory triggering, either by means of navigator or bellows control. When successfully implemented, such a technique results in high-quality images with good anatomic detail (Fig 3).

It has been shown that respiratory-triggered DW MR imaging improves liver detection, compared with breath-hold DW MR imaging (sensitivity for lesion detection, 93.7% vs 84.3%) (57), and improves image quality, SNR, and ADC quantification (54). However, the implementation of respiratory triggering increases the acquisition time (approxi-mately 5–6 minutes), as the images are only acquired in part of the respiratory cycle. The longer acquisition time can increase the chance of patient movement in the imager. Last but not least, there is a risk of pseudo-anisotropy artifact with use of respiratory triggering, which induces errors in the ADC calculation, especially in noncirrhotic livers (58). Interestingly, it has been found that there was no significant difference in the mean ADC values obtained by using free-breathing or respiratory triggered acqui-sition schemes, although there was less scattering of ADC values associated with respiratory triggering schemes (59). A recent study (60) in volunteers has shown that the ADC values obtained by using the free-breathing technique were more reproducible compared with those obtained by using breath-hold or navigator controlled image acquisitions (see ADC quantification section for discussion on sources of variability).

In the left lobe of the liver, cardiac motion results in spin dephasing, which causes artifacts. Such artifacts are worse at higher b values and when breath-hold imaging is used and can result in spuri-ously high ADC values over the left hepatic lobe (61). One way of minimiz-ing such artifact is to use pulse (62) or
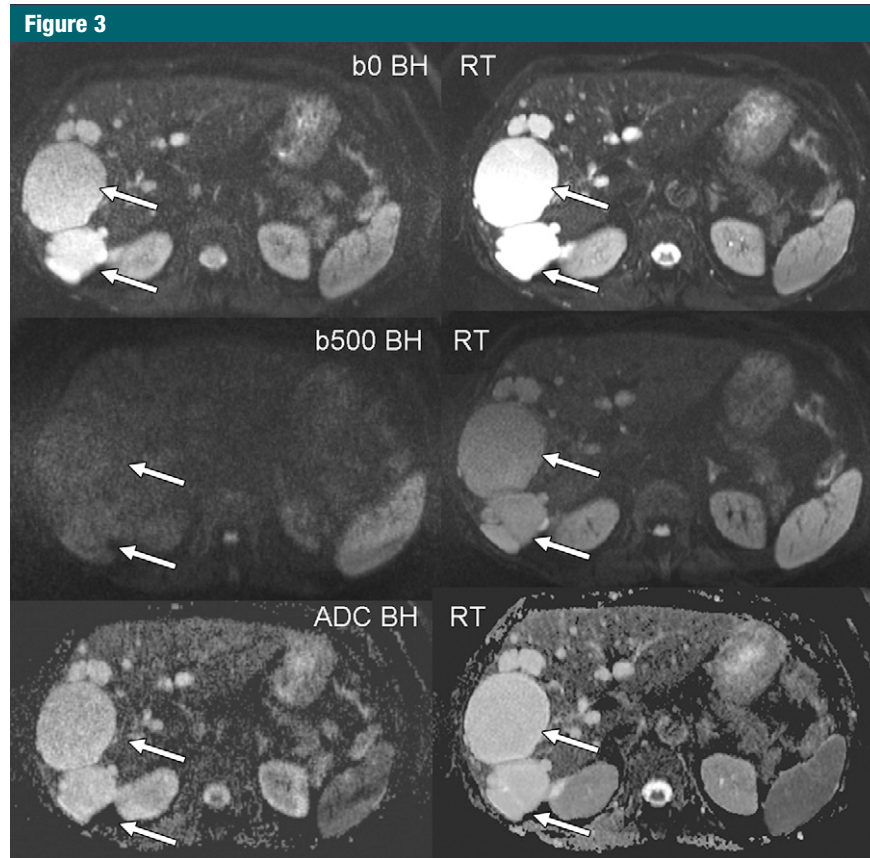
Figure 3

Figure 3: Transverse breath-hold (*BH*) versus respiratory-triggered (*RT*) fat-suppressed single-shot SE echo-planar diffusion acquisition in a 78-year old woman with liver cysts. Respiratory-triggered acquisition (using navigator echo, four signals acquired) shows better image quality at *b* of 0 and 500 sec/mm^2 (with better lesion delineation) and more homogeneous ADC maps compared with breath-hold acquisition (two signals acquired). There is strong signal decrease of liver cysts (arrows), with corresponding high ADC values (approximately 2.9–3 × 10^{-3} mm^2/sec).

cardiac triggering (55) at image acquisition. However, the use of pulse or electrocardiogram-triggered acquisitions can be difficult to implement. Furthermore, cardiac triggering also increases the measurement time, and combining the use of respiratory and cardiac triggering can substantially prolong the examination time for up to six times as long compared with free-breathing non-triggered acquisitions.

Not surprisingly, the choice of DW MR imaging technique in the liver in clinical practice is likely to be influenced by the MR imaging platform, local expertise, physics support, and available examination time. In our opinion, breath-hold DW MR imaging may be appropriate in a time-pressured environment, whereas a free-breathing re-spiratory triggered acquisition may be desired in a research setting. It is important to remember that each of these techniques has its inherent trade-offs and the radiologists should be aware of these when they are applied. Suggested image acquisition schemes using breath-hold and non– breath-hold techniques (as used in the author's institutions) are summarized in Table 1.

Choice of b Values and Sequence Optimization

Because of the relatively short T2 relaxation time of the normal liver parenchyma (approximately 46 msec at 1.5 T and 24 msec at 3.0 T) (63), the *b* values used for clinical imaging are typically no higher than 1000 sec/mm^2. To generate *b* values larger than this would generally require the use of longer diffusion-gradient pulses with longer echo times and thus being prone to loss of signal from T2 decay. Applying a small diffusion weighting of *b* less than 100–150 sec/mm^2 nulls the intrahepatic vascular signal, creating the so-called black-blood images, which improves detection of focal liver lesions (Fig 4) (52,57,64,65), while higher *b* values (≥ 500 sec/mm^2) give diffusion information that helps focal liver lesion characterization (35,44). Hence, when performing DW MR imaging in the liver, it is advantageous to perform imaging by using both lower and higher *b* values (eg, *b* = 0, *b* ≤ 100, and *b* ≥ 500 sec/mm^2. Additional *b* values can be considered in the context of research, clinical trials, or when the primary aim is to obtain an accurate ADC (eg, for the assessment of liver cirrhosis), since increasing the number of data points can reduce the error in the ADC estimation. To ensure that the highest quality images are consistently obtained, the imaging sequences should be optimized to maximize SNR and reduce artifacts, which may arise from motion, eddy currents, chemical shift, Nyquist ghosting, susceptibility effects (66), and noise amplification from acceleration techniques (referred to as the g factor, which relates to the amplification of noise in a parallel imaging study) (67). A full discussion of sequence optimization is beyond the scope of this review and the readers may want to refer elsewhere (17). However, the broad principles are briefly discussed in the Limitations section.

Image Display and Processing

Trace diffusion images (average images between the images obtained with the three diffusion-gradient directions) are displayed for each *b* value acquired, together with an ADC map. High-*b*-value images are assessed for areas of restricted diffusion, appearing as high signal intensity. The grayscale may be inverted to yield images that superficially resemble positron emission tomographic (PET) scans, as described by Takahara et al (68), who have investigated the use of a short inversion time inversion-recovery echo-planar imaging diffusion

Table 1

Suggested Sequence Parameters for Performing Diffusion-weighted MR Imaging of the Liver

Parameter	Breath-hold Acquisition	Free-breathing or Respiratory-triggered Acquisition
Field of view (right-left × anteroposterior in mm)	350–400 × 262–300	350–400 × 262–300
Matrix size (phase × frequency encoding)	144 × 192	144 × 192
Repetition time	≥ 1600–2000	2500–6000
Echo time*	Minimum (~71)	Minimum (~71–82)
Echo-planar imaging factor†	144	144
Phase-encoding direction	Anteroposterior	Anteroposterior
Parallel imaging acceleration factor	2	2
Number of signals acquired	2	≥ 5
Section thickness (mm)	7–8	5–7
Number of sections	10	20
Direction of motion probing gradients‡	Phase, frequency, and section (trace§)	Phase, frequency, and section (trace§)
Fat suppression	Yes	Yes
b Values (sec/mm^2)	0, 50–100, 500	0, 50–100, 500, 700–1000
Acquisition time	23 sec	2–3 min (free breathing), ≥ 3 min (respiratory triggering)

*Minimum echo time depends on the system and the b values used and should be kept fixed for all b values used in a study.

†Number of k-space lines collected per number of signals acquired.

‡Three directions are generally used for liver imaging, although more directions could be used (diffusion-tensor imaging) (8,14,21,26–30).

§ Trace is the average image from three directions.

sequence with background suppression using a high b value in the neck, chest, and abdomen. Fusion imaging is not frequently utilized for liver assessment. However, by using a false color scale to display DW MR imaging or ADC information, the unique information derived from a diffusion-weighted sequence could be overlaid on a conventional grayscale T1- or T2-weighted images. It is worthwhile to note that a false color scale may introduce artificial segmentation on an image, and this should be borne in mind when applying such technique. ADC calculation from the native b value images is a semiautomated process on most commercial MR imagers or workstations. However, more sophisticated analyses may be possible off-line by using developmental software to apply more complex algorithms to the data fitting (eg, biexponential models based on IVIM) (36,69,70). ADCs calculated by omitting lower b values (eg, < 200 sec/mm^2) are perfusion insensitive (39,42). This is relatively easy to perform and is increasingly used in research studies.

Qualitative visual assessment.—Visual assessment is helpful for disease detection and characterization by observing the differential signal attenuation between tissues on DW MR images. Cellular tissues, such as tumors or abscesses, will demonstrate restricted diffusion (high signal intensity) on higher b value (≥ 500 sec/mm^2) images and lower ADC values. By contrast, cystic or necrotic tissues will show a greater degree of signal attenuation on higher b value diffusion images and return higher ADC values (Figs 2, 3, 5, 6). However, the signal intensity observed on the diffusion image is dependent on both water proton diffusivity and the tissue T2-relaxation time, which is a possible confounding factor. This means that a lesion may appear to show restricted diffusion on DW MR images because of the long T2-relaxation time rather than the limited mobility of the water protons (T2 shine-through). This phenomenon can be observed in the normal gallbladder, cystic lesions, and hemangiomas. The presence of T2 shine-through is recognized by correlating high-b-value images with the ADC map. Areas demonstrating substantial T2 shine-through
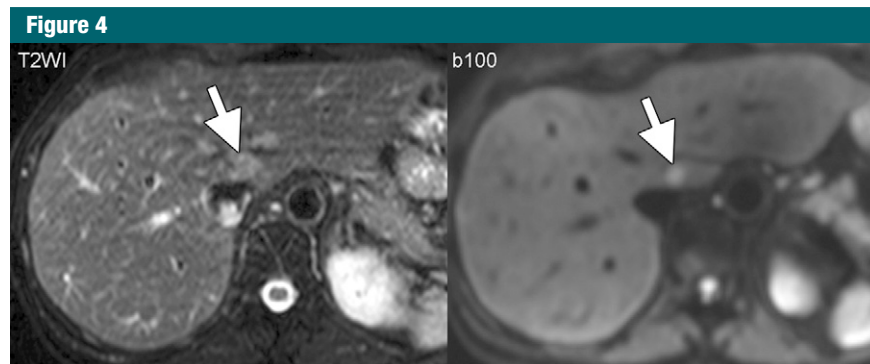
Figure 4

Figure 4: Lesion detection with DW MR imaging versus T2-weighted imaging. Transverse fat-suppressed (left) turbo SE T2-weighted image and (right) single-shot SE echo-planar diffusion image ($b = 100$ sec/mm^2) in a 54-year-old man with colorectal cancer. Application of diffusion weighting with small b value eliminates the high signal intensity from the intrahepatic vasculature, which makes the metastasis (arrows) in the caudate lobe of the liver more conspicuous on DW MR image than on T2-weighted image.
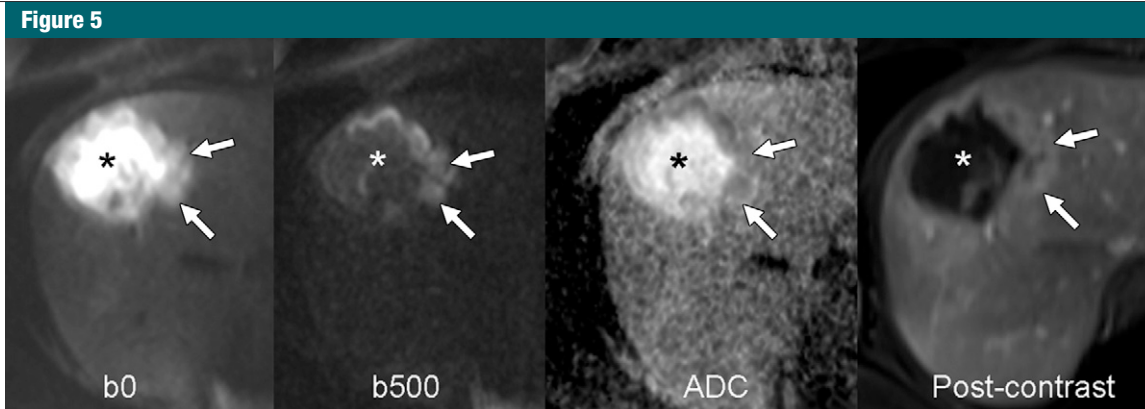
Figure 5: Necrotic breast cancer metastasis. Transverse fat-suppressed breath-hold single-shot SE echo-planar diffusion images obtained by using b values of 0 and 500 sec/mm^2 with corresponding ADC map and postcontrast image in a 43-year-old woman with breast cancer treated with chemotherapy. The higher signal intensity necrotic center of the tumor on image obtained with b of 0 sec/mm^2 shows greater signal attenuation on the image obtained with b of 500 sec/mm^2, with higher ADC (*) compared with the cellular enhancing rim, which has restricted diffusion and lower ADC (arrows).
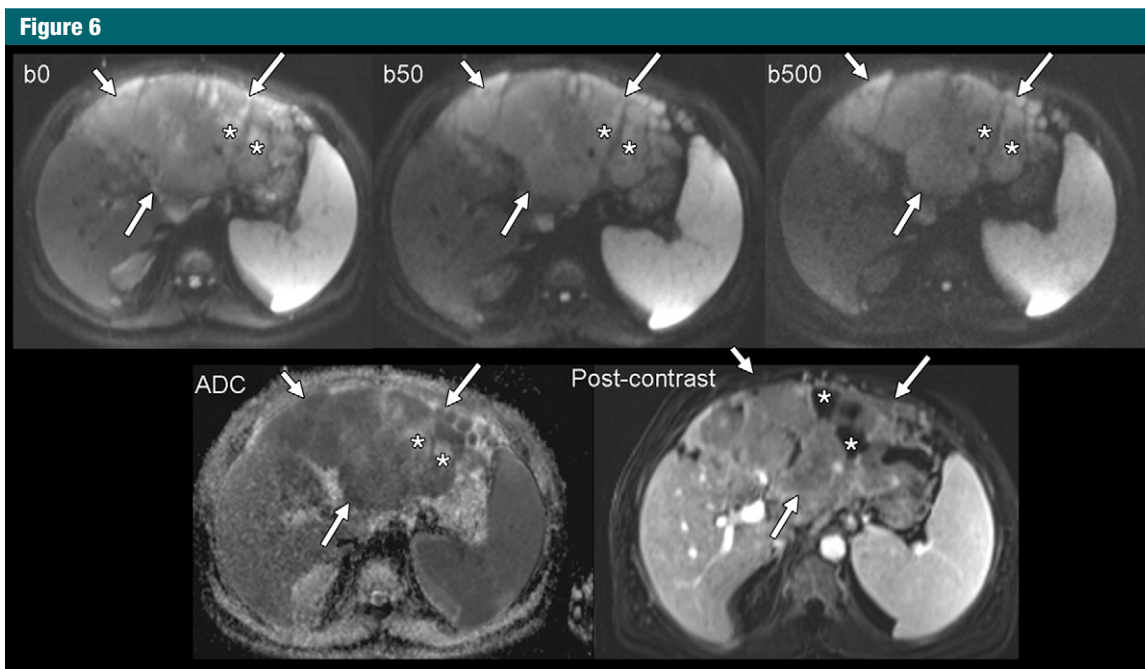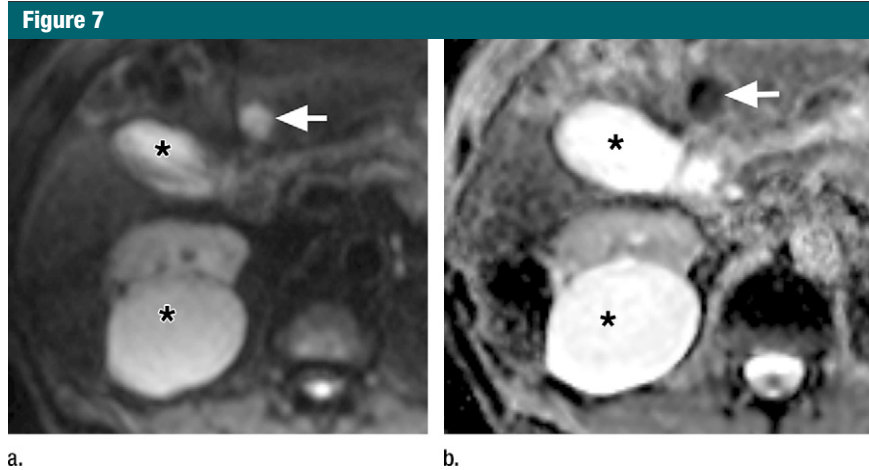

Figure 6: HCC after chemoembolization. Transverse fat-suppressed breath-hold single-shot SE echo-planar diffusion images ($b = 0$, 50, and 500 sec/mm^2) with corresponding ADC map and subtracted postcontrast image in a 56-year-old man with cirrhosis and large infiltrative HCC of the left hepatic lobe (arrows) treated with chemoembolization. The lesion shows restricted diffusion, except for a smaller portion, which is necrotic after treatment (*).

rather than restricted diffusion will show high diffusivity on the ADC map and high ADC values (Figs 7, 8). For this reason, diffusion images should be interpreted concurrently with the ADC map and all other available morphologic imaging to prevent misinterpretation.

Quantitative assessment.—The ADC of the liver calculated from diffusion acquisition can be appraised by either visual assessment of the ADC maps or by drawing regions of interest on the ADC maps to record the mean or median ADC values in the tissue of interest. ADC is usually expressed ($\times 10^{-3}$) as square millimeters per second and is being investigated by several research groups as an index for assessing tumor response to treatment. The ADC can also aid in the characterization of liver lesions and for the diagnosis of liver fibrosis

Radiology

Figure 7

a.   b.

Figure 7: T2 shine-through effect with DW MR imaging. **(a)** Transverse fat-suppressed breath-hold single-shot SE echo-planar diffusion image ($b = 500$ sec/mm²) and **(b)** corresponding ADC map in 60-year-old woman with metastatic liver disease. The liver metastasis (arrow), renal cyst, and gallbladder (∗) show high signal intensity on **a**. This is clarified on **b**, where the metastasis shows low diffusivity reflected by the low ADC, while the cyst and gallbladder show high ADC, not because of restricted water diffusion, but because of the long T2 relaxation time of the fluid (T2 shine-through).

and cirrhosis. However, ADC quantification requires minimum acceptable SNR at higher b values (71). Use of low-SNR images for ADC quantification may artificially reduce the ADC.

ADC Reproducibility

One of the critical issues to ensure consistent and widespread application of quantitative ADC measurements for disease characterization and tumor response assessment is the knowledge of ADC measurement reproducibility and interimager variability. ADC can vary as a result of hardware or human or biologic factors. Even when the same MR system is used, DW MR imaging studies have inherently lower SNR and are susceptible to a range of artifacts, which could increase the variability of the calculated ADC. An even greater degree of variability is to be expected

when comparing ADC measurements across MR platforms, since the MR systems from different vendors will have slightly differing implementation of image acquisition schemes, gradient performance, and artifact reduction strategies. In a recent study (72) assessing intra- and interimager ADC measurement variability of the normal brain in a group of volunteers by using comparable diffusion protocols on different MR platforms across institutions, it was found that the intravendor ADC measurement variability was 4%–9% and the intervendor variability was approximately 7%. Such intra- and interimager variations suggest the need for greater standardization of imaging parameters to minimize the measurement variability across platforms in order to allow more meaningful comparison of results and facilitate multicenter studies (73). Compared with diffusion studies in the brain, performing DW MR imaging in the liver is more challenging because of motion and lower T2. Consequently, there is likely to be a greater degree of error associated with ADC measurements in the liver than in the brain. There are emerging data for measurement reproducibility of ADC measurements in the liver at both 1.5 T (60) and 3.0 T (51), but clearly more research in this area should be encouraged.

Current Applications of Liver DW MR Imaging: Liver Lesion Detection

Comparison with T2-weighted imaging.— Several publications have reported the use of DW MR imaging for liver lesion detection (57,61,64,74–79). Few of these studies have compared DW MR imaging and T2-weighted imaging in terms of lesion detection, generally showing improved detection with DW MR imaging (64,76,78,79); in terms of image quality, findings showed comparable image quality with that of DW MR imaging by using low b values (52,65). Black-blood diffusion images (using low b values), in which background signal of vessels in the liver parenchyma is suppressed, allow for lesion detection (52,64,65), while images with higher b values give diffusion information that enable lesion characterization (35,44,57).

Figure 8

	b0	High b	ADC
Benign Lesion (E.g. cystic-necrotic lesion)	○	●	○
Malignant Lesion (E.g. Metastasis)	○	○	●
T2 shine through (E.g. cyst-hemangioma)	○	○	○

Figure 8: Visual liver lesion characterization with DW MR imaging. This figure gives a simplified approach to lesion characterization by using visual assessment with b of 0 sec/mm² and a higher b value and ADC maps. A benign fluid-containing lesion shows strong signal decrease with high ADC, whereas a cellular malignant lesion shows no or minimal signal decrease, with low ADC compared with the surrounding liver parenchyma. A lesion with long T2 can sometimes show a T2 shine-through effect (see text for explanations). Black circles = hypointense, white circles = hyperintense.
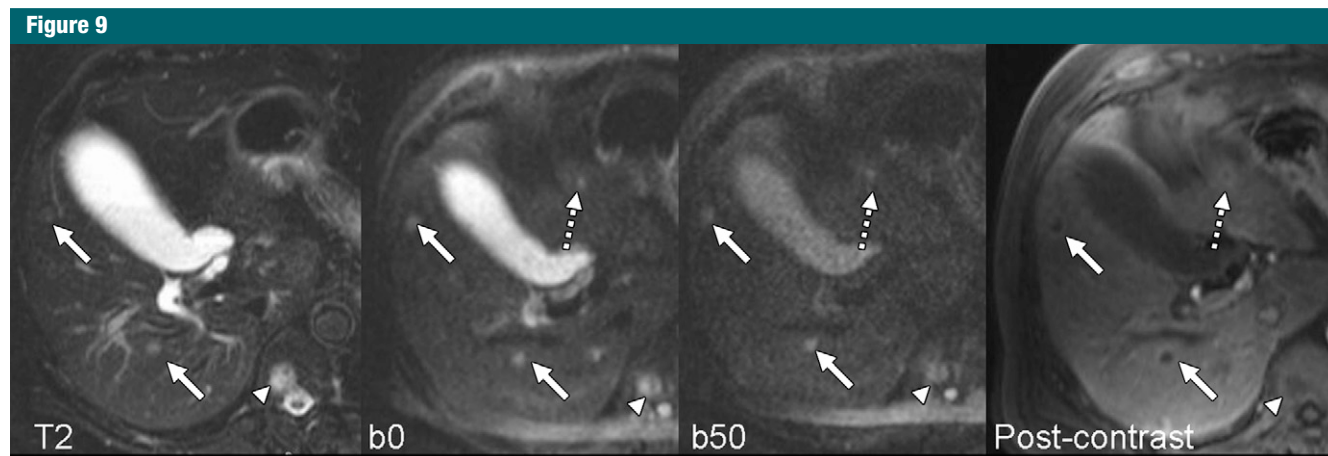
The improved lesion detection with DW MR imaging compared with T2-weighted imaging is explained by the improved image contrast with use of low b values and lack of blurring with single-shot SE echo-planar imaging, compared with T2-weighted fast SE or single-shot fast SE sequences (65). Coenegrachts et al (76) compared DW MR imaging (b values of 0, 20, 300, and 800 sec/mm²) and single-shot T2-weighted fast SE in 24 patients with focal liver lesions. They found that the best image quality was achieved with single-shot T2-weighted fast SE imaging and the best lesion conspicuity was achieved with single-shot T2-weighted fast SE imaging for cysts and with DW MR imaging (b = 20 sec/mm²) for hemangiomas and metastases. DW MR imaging had the highest lesion-to-liver contrast-to-noise ratio for hemangiomas and metastases. In another study, Bruegel et al (78) compared respiratory-triggered DW MR imaging to five different T2-weighted sequences (breath-hold fat-suppressed single shot T2-weighted fast SE, breath-hold fat-suppressed fast SE, respiratory-triggered fat-suppressed fast SE, breath-hold short inversion time inversion recovery, and respiratory-triggered short inversion time inversion recovery) for the diagnosis of hepatic

metastases in 52 patients with 118 lesions at 1.5T. DW MR imaging demonstrated higher accuracy (0.91–0.92) compared with T2-weighted fast SE techniques (0.47–0.67). These differences were even more pronounced for small metastatic lesions (≤ 1 cm). Zech et al (79) compared black-blood DW MR imaging (b = 50 sec/mm²) with fat-suppressed T2-weighted imaging and observed significantly better image quality, fewer artifacts, and better sensitivity for lesion detection with DW MR imaging (83% versus 61%). Black-blood DW MR imaging has also been recently proposed as an alternative to T2-weighted imaging at 3.0 T, giving comparable image quality, improved suppression of fat and blood signals, high contrast-to-noise ratio and SNR, and lower specific absorption rate in a single breath hold (52). Our experience in 53 patients with 211 lesions is similar (57), also showing that DW MR imaging performs better ($P < .001$) than standard breath-hold T2-weighted imaging for lesion detection with a b value of 50 sec/mm², with a respective sensitivity of 87.7% versus 70.1% for detection of all lesions and of 86.4% versus 62.9% for detection of malignant lesions (Figs 4, 9). In addition, DW MR imaging significantly improved

detection of small malignant lesions (< 2 cm) when compared with breath-hold T2-weighted imaging (78.5% vs 45.8%, $P < .001$).

Comparison with contrast-enhanced MR imaging.—In the past few years, liver-specific contrast media usage has become more widespread. Experience with both negative (eg, superparamagnetic iron oxides [SPIOs]) (61,80–82) and positive (eg, mangafodipir trisodium, gadoxetic acid) (83–87) liver-specific contrast media has shown the potential for higher lesion detection rate with use of these agents compared with nonselective extracellular gadolinium chelates. More recently, the diagnostic accuracy of DW MR imaging in detection of liver metastases has been compared with liver-specific contrast media. The use of DW MR imaging in place of gadolinium chelates is very attractive in patients with severe renal dysfunction at risk for nephrogenic systemic fibrosis (9,11,12).

In one study (61), DW MR imaging was found to be more sensitive than SPIO-enhanced MR imaging in detection of colorectal hepatic metastases. SPIO-enhanced MR imaging was less sensitive for metastases of less than 1 cm in diameter; whereas DW MR imaging was less sensitive over the left

Figure 9

Figure 9: Lesion detection with DW MR imaging versus T2-weighted imaging. Transverse fat-suppressed breath-hold T2-weighted image, single-shot SE echo-planar diffusion images (b = 0 and 50 sec/mm²), and postcontrast T1-weighted image in a 65-year-old man with metastatic liver disease from pancreatic cancer. Two small lesions in the right posterior lobe (solid arrows) are identified on T2-weighted and DW MR images; however, an additional small lesion (dashed arrows) is more conspicuous on DW MR image and is confirmed on postcontrast image. There is also a vertebral metastasis (arrowheads).

lobe of the liver due to cardiac motion–related artifacts. Other studies postulated the advantages of combining DW MR imaging with SPIO-enhanced imaging in the liver, since contrast media uptake within benign lesions containing Kupffer cells may improve the diagnostic accuracy DW MR imaging (88,89). For example, Naganawa et al (88) showed that the addition of SPIO contrast medium to DW MR imaging improved the contrast-to-noise ratio of malignant focal liver lesions, thus improving the diagnostic specificity. In a subsequent study (90) comparing SPIO-enhanced with nonenhanced DW MR imaging, better lesion conspicuity, image quality,

and diagnostic sensitivity were achieved with the nonenhanced DW MR imaging technique. However, it was reported that SPIO-enhanced MR imaging was inadequate in distinguishing between benign and malignant solid hepatic lesions, since both types of lesions can show high signal intensity on the SPIO-enhanced DW MR imaging studies.

For the evaluation of colorectal hepatic metastases, one view suggests that it is the addition of DW MR imaging to morphologic imaging using liver-specific contrast medium that improves lesion detection. In one study (77), addition of DW MR imaging to mangafodipir trisodium–enhanced MR imaging sig-

nificantly improved the diagnostic accuracy for detection of colorectal liver metastases compared with either technique alone. DW MR imaging was found to be of value in detecting small (< 1 cm) metastases that mimicked intrahepatic vasculature and also in revealing lesions close to the edge of the liver, as these lesions are easily overlooked on mangafodipir trisodium–enhanced T1-weighted MR images (77) (Fig 10).

Data on the performance of DW MR imaging compared with gadolinium-enhanced sequences for liver lesion detection are still lacking. To our knowledge, there is only one published study (75) directly comparing DW MR imaging with gadolinium-pentetic acid MR imaging for tumor detection, showing improved detection of liver lesions compared with conventional MR imaging, including postcontrast sequences (Fig 11).

To summarize, there are compelling data that show better performance of DW MR imaging compared with T2-weighted imaging for lesion detection. In addition, even if more data demonstrating the added value of DW MR imaging over contrast-enhanced imaging are needed, we believe that the combination of DW MR imaging with conventional sequences (including T2-weighted and contrast-enhanced sequences) may potentially improve the diagnostic accuracy of conventional imaging alone for liver lesion detection and characterization. As such, we suggest that DW MR

Figure 10

a.   b.
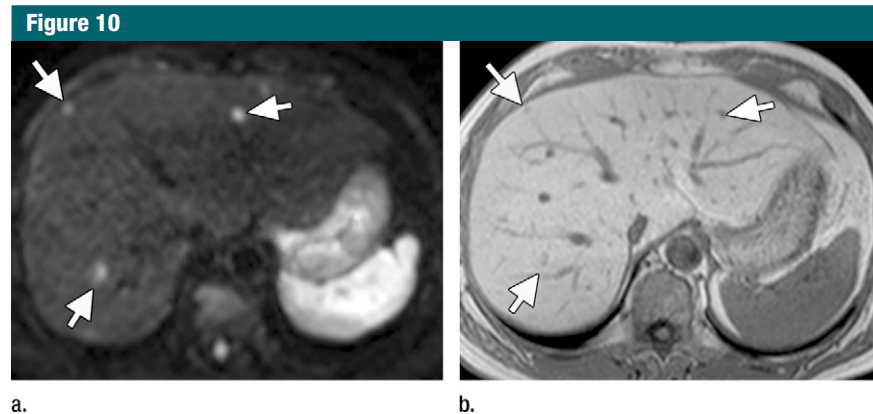
Figure 10: Lesion detection at DW MR imaging versus mangafodipir trisodium–enhanced T1-weighted imaging. **(a)** Free-breathing transverse single-shot SE echo-planar DW MR image ($b = 750$ sec/mm^2) and **(b)** mangafodipir trisodium–enhanced T1-weighted image in a 47-year-old man with colorectal cancer. The small metastatic lesions (arrows) show high conspicuity on **a**, and these are easy to overlook on **b** due to their perivascular or subcapsular locations.
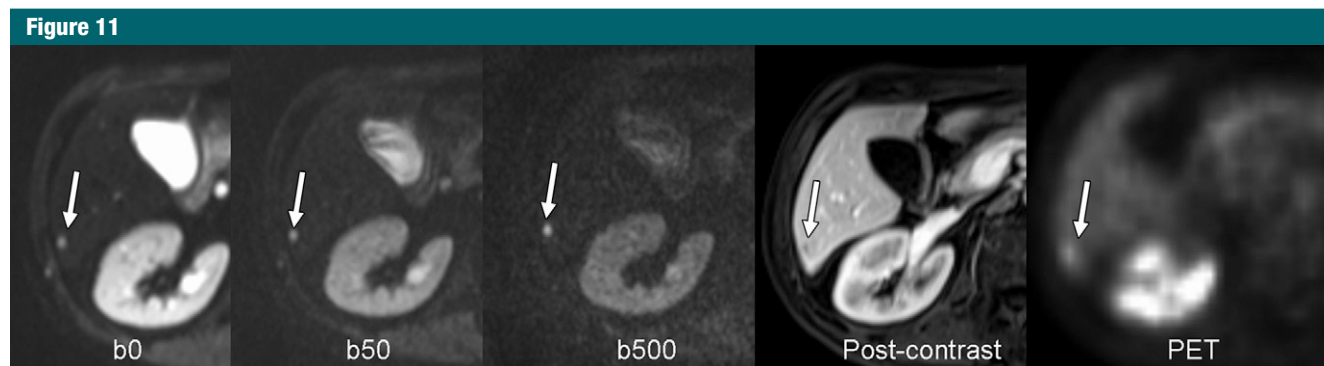
Figure 11

Figure 11: Lesion detection at DW MR imaging versus gadolinium-DTPA-enhanced T1-weighted imaging. Breath-hold transverse single-shot SE echo-planar DW MR images ($b = 0$, 50, and 500 sec/mm^2), postcontrast T1-weighted image, and PET scan in a 56-year-old man with lung cancer. There is a tiny metastatic lesion of segment 6 (arrows) not identified prospectively at contrast-enhanced T1-weighted imaging and is more conspicuous at DW MR imaging. The lesion was confirmed at fluorodeoxyglucose PET performed immediately after MR imaging.

Radiology

Table 2

Mean ADCs of Normal Liver and Focal Liver Lesions, ADC Cutoffs, and Sensitivity and Specificity for Diagnosing Malignant Lesions as Reported in Selected Studies

Parameter	Namimoto et al (125)	Kim et al (44)*	Taouli et al (35)†	Bruegel et al (45)	Gourtsoyianni et al (46)	Parikh et al (57)
No. of patients/lesions	51/59	126/79	66/52	102/204	38/37	53/211
b Values (sec/mm^2)	30, 1200	≤ 846	≤ 500	50, 300, 600	0, 50, 500, 1000	0, 50, 500
ADC values						
Normal liver	0.69	1.02	1.83	1.24	1.25-1.31	Not applicable
Metastases	1.15	1.06–1.11	0.94	1.22	0.99	1.50
HCCs	0.99	0.97–1.28	1.33	1.05	1.38	1.31
Hemangiomas	1.95	2.04–2.10	2.95	1.92	1.90	2.04
Cysts	3.05	2.91–3.03	3.63	3.02	2.55	2.54
Adenomas- focal nodular hyperplasias	Not applicable	Not applicable	1.75	1.40	Not applicable	1.49
Benign lesions	1.95	2.49	2.45	Not applicable	2.55	2.19
Malignant lesions	1.04	1.01	1.08	Not applicable	1.04	1.39
ADC cutoff for diagnosis of malignant liver lesions‡	Not applicable	1.60	1.50	1.63	1.47	1.60
Sensitivity (%)	Not applicable	98	84	90	100	74
Specificity (%)	Not applicable	80	89	86	100	77

* ADCs for $b < 850$ sec/mm^2 are given.

† ADCs for $b = 0–500$ sec/mm^2 are given.

‡ Lesions with ADC below the proposed cutoff value are considered malignant, while those with ADC above are considered benign.

imaging should be fully integrated in routine liver MR protocols.

Current Applications of Liver DW MR Imaging: Liver Lesion Characterization

Role of visual assessment.—Visual assessment of DW MR images, which includes those with higher b values (≥ 500 sec/mm^2), can help to distinguish between solid and cystic lesions. While simple cysts typically show suppression of high signal intensity at higher b values (Figs 2, 3), T2 shine-through may occasionally be encountered (91). As a general observation, both benign and malignant solid lesions may demonstrate residual high signal intensity on higher b value images and would be difficult to characterize with visual assessment of the DW MR images alone. Hence, once a cellular hepatic lesion is identified visually, further characterization usually relies on conventional morphologic (with or without contrast enhancement) imaging, supplemented with ADC measurements. Specifically, in malignant lesions, DW MR imaging is useful in distinguishing the different components of tumors (cystic

and/or necrotic vs solid components). On visual inspection of diffusion images alone, false-positive identification of malignant disease may result from T2 shine-through, partial volume effects from adjacent structures, and cellular benign lesions (eg, focal nodular hyperplasia, adenoma, and abscess). False-negative findings may result from metastases arising from mucinous tumors, which can mimic the appearance of a cyst, well-differentiated tumors (eg, well-differentiated hepatocellular carcinoma [HCC]), necrotic lesions (either primarily necrotic or secondary to treatment) (Figs 5, 6), and image artifacts, which could obscure lesion visualization. In our experience, lesion characterization as benign or malignant was correct in 89% of lesions using DW MR imaging with visual assessment (57).

Role of ADC quantification.—Benign hepatic lesions have generally higher ADC values compared with malignant lesions, with variable degree of overlap (35,39,43–46,57,78,92–94). Different ADC cutoffs (1.4–1.6 × 10^{-3} mm^2/sec) have been described in the literature, with a reported sensitivity of 74%–100%

and specificity of 77%–100% (Table 2) for diagnosing malignant lesions. The ADCs of various benign and malignant hepatic lesions from selected published studies are summarized in Table 2.

The variation in ADC cutoffs is due to differences in the DW MR imaging technique applied for image acquisition, the choice of b values, and the liver lesions assessed (35,39,43–46, 57,78,92–94). The diagnostic performance of DW MR imaging reported in the study by Parikh et el (57) (area under the curve, sensitivity, and specificity of 0.839, 74%, and 77%, respectively) likely reflects the realistic performance of ADC, since it assessed the largest number of various benign and malignant lesions (including solid benign lesions and abscesses) and included treated malignant lesions, which may lower the accuracy of ADC. An important source of variability in ADC measurement is the b value(s) used for image acquisition. As explained above, microcapillary perfusion (or pseudo-diffusion phenomenon) can affect the ADC values of liver lesions (excluding cysts) when lower b values are used
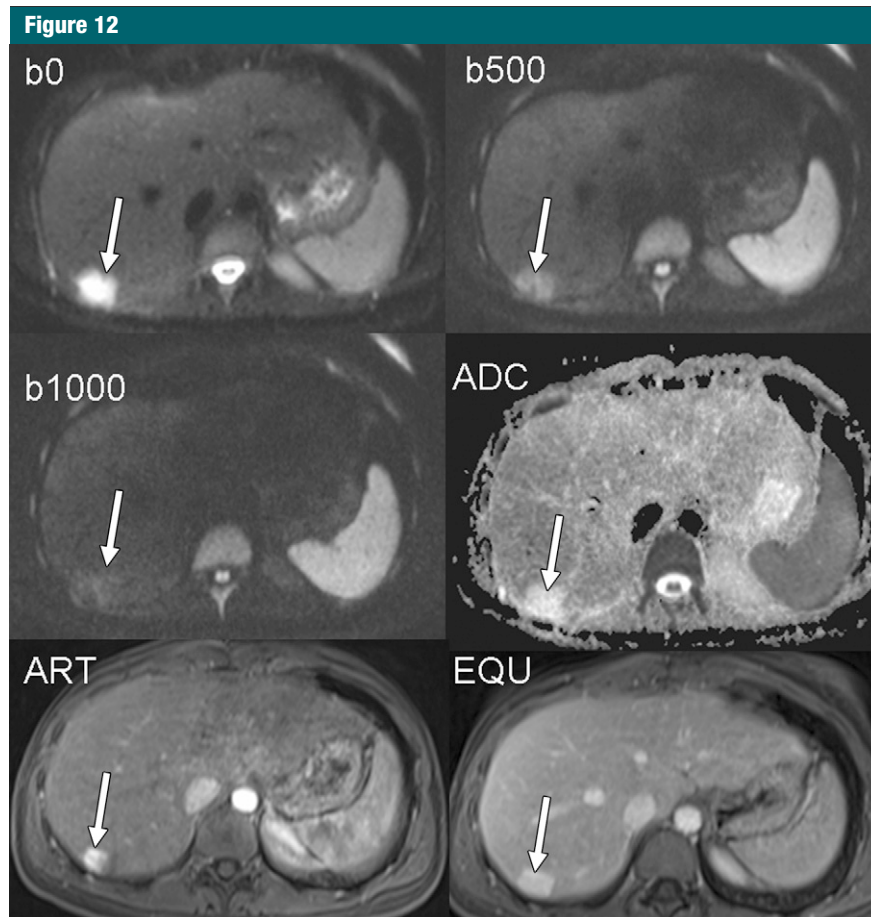
Figure 12

Figure 12: Lesion characterization with DW MR imaging. Transverse breath-hold single-shot SE echo-planar DW MR images ($b = 0$, 500, and 1000 sec/mm^2), postcontrast T1-weighted images during arterial phase (*ART*) and equilibrium phase (*EQU*), and ADC map in a 44-year-old woman with hemangioma (arrows) of the right hepatic lobe. The lesion is bright at b of 0 sec/mm^2 and attenuates progressively with increasing b values, with corresponding high ADC (2.8×10^{-3} mm^2/sec). Postcontrast images show early and persistent enhancement.

(38,39,43,44), compared with ADCs obtained with higher b values (35,45–47). Hence, ADC thresholds applied for lesion characterization should be derived from imaging studies using similar techniques and ranges of b values for meaningful interpretation.

Furthermore, since there can be substantial overlap in the range of ADCs between different pathologies, the ADC should be interpreted concurrently with all available imaging before making the radiologic diagnosis. Simple liver cysts have very high ADC values due to their fluid content (Figs 2, 3). Hemangiomas usually demonstrate high ADC values, but lower than those of cysts (Fig 12)

(35,45,94–96). Focal nodular hyperplasias and adenomas have intermediate ADC values that can overlap with those of malignant lesions and normal liver parenchyma (35,45,57,94). For example, ADCs of focal nodular hyperplasias and adenomas were reported to range from 0.96 to 3 x 10^{-3} mm^2/sec (using 0–500 sec/mm^2) (35). Liver abscesses return lower ADC values due to cellular debris and exudates, which distinguishes them from cystic or necrotic tumors (97). Malignant lesions such as HCC and liver metastases usually display low ADC values, except when treated and/or necrotic (Figs 2, 5, 6, 13, 14). Hepatic metastases that demonstrate sub-

stantial central necrosis can demonstrate high ADCs (Figs 5, 13) (47). In comparison, liver metastases that arise from neuroendocrine tumors, which are characterized by small round cells at histologic examination, have low ADC values (Fig 14) (94). HCCs may be difficult to differentiate from surrounding cirrhotic changes or dysplastic nodules, as these can have similar ADC values (35,39,94,98,99).

To summarize, it is important to remember that DW MR imaging is a marker of cellularity, and as such, benign solid lesions (focal nodular hyperplasia and adenomas) may sometimes display restricted diffusion. On the other hand, necrotic malignant lesions can demonstrate high ADC values.

DW MR Imaging in Assessment of Tumor Response to Treatment

DW MR imaging is increasingly applied to evaluate tumor response to chemotherapy, radiation therapy, and local ablation (17,100). Studies in both animals and humans have shown that effective tumor treatment results in an increase in the ADC value, which can occur prior to any measurable change in tumor size (101). Transient reduction in ADC within 24–48 hours after initiation of treatment has been observed, hypothesized to result from acute cell swelling or possibly reduction of interstitial volume (102). Following the increase in ADC with treatment, the ADC will subsequently decrease, which is related to tumor repopulation, fibrosis or tissue remodeling, and decreased perfusion (17,103,104).

Understanding DW MR imaging response in preclinical models.—DW MR imaging experiments have been conducted in different animal models to understand the mechanistic changes in tumors in response to chemoradiation and minimally invasive therapy. The rabbit VX-2 tumor model is one of the most widely studied (105–110). Tumor necrosis corresponded to higher ADC values compared with viable tumor (102,106). Chemoembolization resulted in an increase in the ADC at 7 days after intervention (108), but tumors with complete necrosis or less than 5% viable
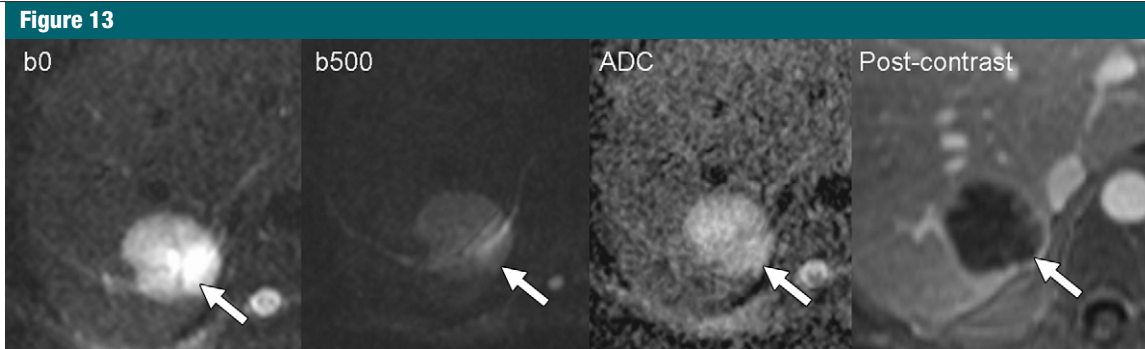
Figure 13: Pitfall of DW MR imaging: necrotic colon cancer metastasis after treatment. Transverse fat-suppressed breath-hold single-shot SE echo-planar diffusion images ($b = 0$ and 500 sec/mm^2) with corresponding ADC map and postcontrast image in a 62-year-old man with metastatic colon cancer treated with systemic chemotherapy. The metastatic lesion is hyperintense at b of 0 sec/mm^2, but shows no diffusion restriction with corresponding high ADC, in relation to its necrotic content, as shown on the postcontrast image.
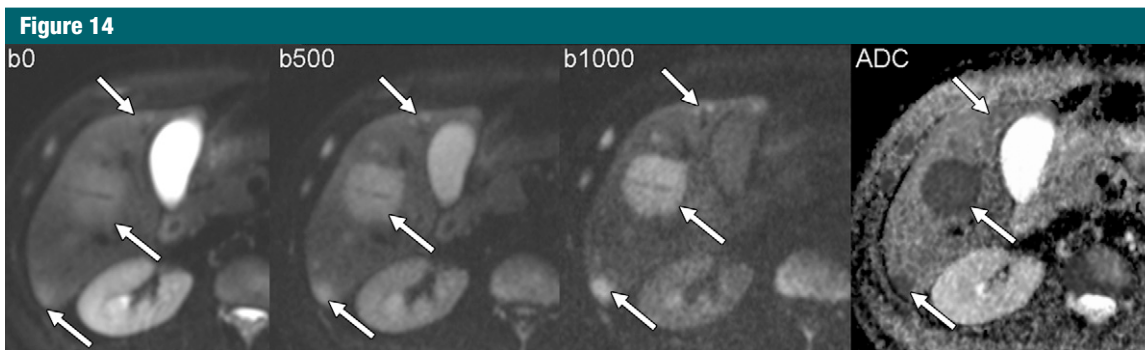
Figure 14: Neuroendocrine liver metastases in a 24-year-old man. Transverse fat-suppressed breath-hold single-shot SE echo-planar diffusion images ($b = 0$, 500, and 1000 sec/mm^2) with corresponding ADC map show multiple lesions with restricted diffusion in the right hepatic lobe (arrows). The largest lesion shows a very low ADC (0.9×10^{-3} mm^2/sec) in relation to tumor cellularity.

tumor could not be distinguished at DW MR imaging (108). Cellular edema with restricted water diffusion was observed in the tumor rim or in the surrounding liver parenchyma at 16–48 hours after chemoembolization (111). More recently, it was shown that the ADC also increased after radiofrequency ablation in treated tumors, which corroborated with a decrease in fluorine 19 fluorodeoxyglucose tracer uptake at PET (110). Insights gained from such animal studies have helped to translate DW MR imaging measurements for evaluating the effects of antitumor treatments to humans.

Human data.—There are limited data on the use of DW MR imaging for prediction of liver metastases response to treatment (112–114). In colorectal hepatic metastases, the mean ADC increased in metastases that showed at least a partial response to chemotherapy according to the Response Evaluation Criteria in Solid Tumors, or RECIST, (Fig 15). This ADC increase was not observed in lesions that showed either no change or disease progression according to the RECIST criteria (90,112). In one study (113), an early increase in ADC at 3–7 days after initiation of chemotherapy was observed among responders but not in nonresponders. Intriguingly, it was reported that colorectal metastases with a high pretreatment ADC responded poorly to chemotherapy, which suggests that tumors that were more necrotic prior to treatment are more chemo-resistant (112,113). Clearly, these findings need to be validated in larger prospective studies, but nevertheless they illustrate the potential predictive value of the imaging technique. The applications of DW MR imaging for evaluating the effects of chemoembolization (114), new therapeutics, and minimally invasive therapies are being investigated, and it is anticipated that the results of many such trials will be made available over the next few years.

The assessment of HCC response to chemoembolization with MR imaging relies on tumor size change, which is a late finding, and on the presence of tumor necrosis and residual enhancement on contrast-enhanced MR images, which can be difficult to evaluate due to the presence of signal intensity changes (hyperintensity on unenhanced T1-weighted images) related to a combination of iodized oil injection and hemorrhagic necrosis (115,116). There are several reports on the use of DW MR imaging to evaluate HCC response to chemo- or radioembolization (117–122).
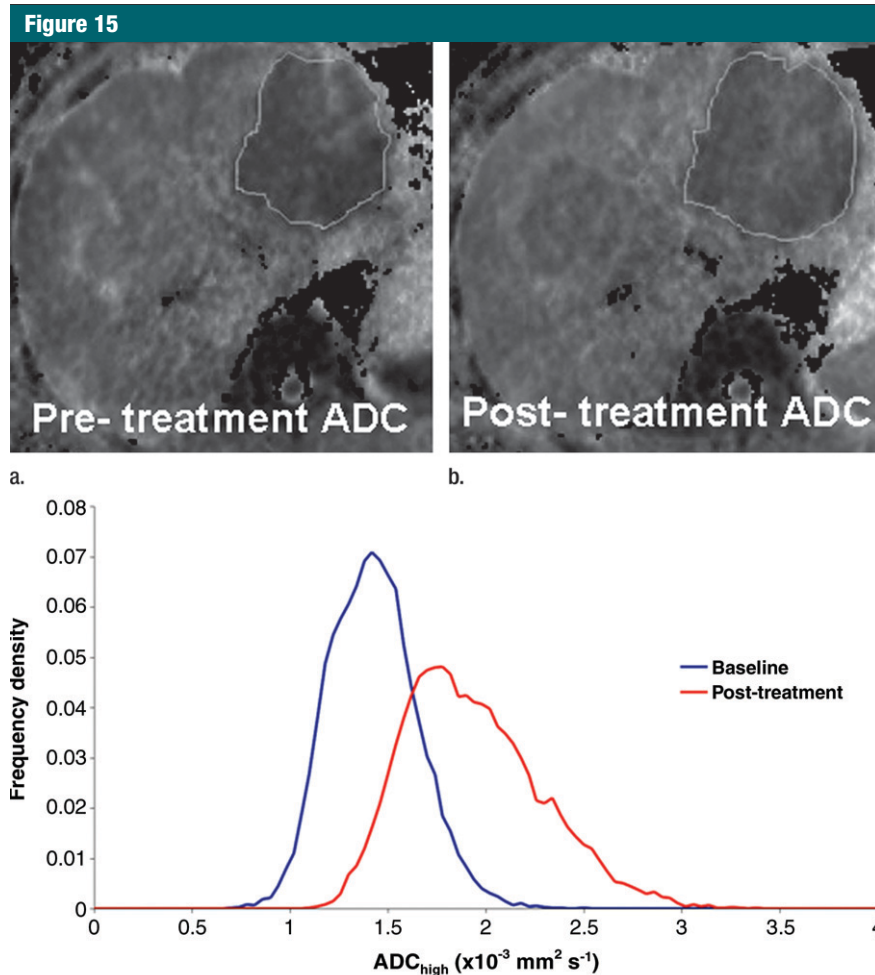
Figure 15

Figure 15: Assessment of treatment response with DW MR imaging. Perfusion-insensitive ADC (ADC_{high}, using b values > 200 sec/mm^2) maps show a metastasis in the left lobe of the liver **(a)** before and **(b)** after treatment with an antiangiogenic agent. **(c)** Voxelwise histogram analysis shows a clear increase in the median ADC_{high} after treatment, with a shift of the histogram toward the right (red line) compared with the pretreatment distribution (blue line). (Image courtesy of Matthew Blackledge, Institute of Cancer Research, Sutton, UK.)

These studies have demonstrated differences in ADC between viable and necrotic portions of HCCs after treatment (Fig 6) and measurable differences before and after treatment. An initial clinical study (117) showed excellent correlation ($r = 0.95$) between ADC and percentage of necrosis at histopathologic examination. In our experience (21 patients with 28 HCCs confirmed at liver explant) (123), ADC had a significant correlation with necrosis as assessed at histopathologic examination ($r = 0.64$, $P < .001$). For prediction of complete tumor necrosis after chemoembolization, we observed an area under the curve of 0.85, sensitivity of 75%, and specificity of 88% with ADC, compared with an area under the curve of 0.82–0.89, 100% sensitivity, and 58%–79% specificity for contrast-enhanced image subtraction, without a significant difference between both techniques (123). There are limited data on the use of DW MR imaging for diagnosing HCC recurrence after transcatheter arterial chemoembolization. A recent study showed lower performance of DW MR imaging compared with contrast-enhanced imaging, with sensitivity for detection of local HCC recurrence of 60.7% compared with 82% for contrast-enhanced imaging (124).

Diagnosis of Liver Fibrosis and Cirrhosis with DW MR Imaging

The diagnosis of fibrosis and inflammation is difficult with conventional MR imaging sequences. Several reports have demonstrated that ADC of cirrhotic liver is lower than that of normal liver (35,43,44,125–127). Koinuma et al (99) evaluated a large ($n = 163$) population of patients, 31 of whom had undergone a liver biopsy, using a low b value (128 sec/mm^2). Their results demonstrated a significant negative correlation between ADC and fibrosis score; however, there was no correlation between ADC and inflammation grades. Lewin et al (128) compared DW MR imaging (using b values of 0, 200, 400, and 800 sec/mm^2) with a sonographic elastography technique (FibroScan; Echosens, Paris, France) and serum markers of fibrosis (including FibroTest; BioPredictive, Paris, France) in 54 patients with chronic hepatitis C and 20 healthy volunteers. They observed excellent performance of ADC for the prediction of moderate and severe fibrosis. Patients with moderate-to-severe fibrosis (stage, F2-F4) had hepatic ADC values lower than those without or with mild fibrosis (stage, F0-F1) and healthy volunteers: (1.10 ± 0.11) $\times 10^{-3}$ mm^2/sec, (1.30 ± 0.12) $\times 10^{-3}$ mm^2/sec, and (1.44 ± 0.02) $\times 10^{-3}$ mm^2/sec, respectively. For the distinction of patients with fibrosis stage F3-F4 from those with stage F0-F2, the areas under the curve were 0.92 for ADC, 0.92 for FibroScan, and 0.79–0.87 for blood tests. Sensitivity and specificity of ADC were 87% and 87%, respectively (ADC cutoff, 1.21×10^{-3} mm^2/sec). In addition, Lewin et al found a significant relationship between ADC and inflammation scores and suspected a possible associated influence of steatosis on ADC values. Girometti et al (129) reported lower ADCs in cirrhotic livers compared with those in healthy controls ($1.11 \pm 0.16 \times 10^{-3}$ mm^2/sec vs $1.54 \pm 0.12 \times 10^{-3}$ mm^2/sec) and showed an area under the curve of 0.96, sensitivity of 92%, specificity of

Table 3

Proposed Strategy to Improve Single-Shot Echo-planar DW MR Imaging Quality of the Liver

DW MR Imaging Limitations	Proposed Solutions
Poor SNR	Longer repetition time (minimun,1400 msec)
	Shorter echo time
	Larger field of view
	Free breathing (increase number of signals acquired)
	Increase section thickness
	Smaller matrix
	Lower b values
	High field
	Smaller bandwidth
Spatial resolution	Thinner sections
	Parallel imaging
Echo-planar imaging artifacts	Parallel imaging
	Pulse trigger (for cardiac motion artifacts)
	Bipolar diffusion gradients

100%, positive predictive value of 100%, negative predictive value of 99%, and accuracy of 96% using ADC cutoff of 1.31×10^{-3} mm^2/sec (b = 0, 150, 250, and 400 sec/mm^2). Another recent study showed the ADC to be a significant predictor of fibrosis stage 1 or greater (sensitivity of 88.5% and specificity of 73.3%) and inflammation grade 1 or greater (sensitivity of 75% and specificity of 78.6%) (32). The same group also showed a decrease in liver ADC in significant and severe fibrosis (fibrosis stage 2 and greater) using b values of 500 sec/mm^2 or greater (130), with the best results demonstrated with a b value of 700 sec/mm^2. In this study, ADC was a significant predictor of fibrosis stage 2 or greater and stage 3 and greater, with an area under the curve of 0.896 and 0.896, sensitivity of 83.3% and 88.9%, and specificity of 83.3% and 80.0%, respectively.

The mechanism of diffusion restriction is probably multifactorial and not completely understood, possibly related to the presence of increased connective tissue in the liver, which is proton poor, and decreased blood flow, as shown in dynamic contrast-enhanced MR imaging studies (131,132). An animal study (133) showed that rats with hepatic fibrosis demonstrated reduced ADC values in vivo but not when DW MR imaging was performed ex vivo, which favors the perfusion effect on diffusion measurement. In a clinical study, Yamada et al (39) used the IVIM model to calculate true diffusion coefficient (D), ADC, and perfusion fraction of the liver parenchyma and liver lesions. They reported lower D values compared with ADC in enhancing lesions and liver parenchyma, confirming that ADC is contaminated by perfusion. They did not report the pseudo-diffusion coefficient ($D*$) in their study. Furthermore, they showed no difference in perfusion fraction and D between cirrhotic and normal livers. Recently, Luciani et al (41) applied the IVIM model to quantify perfusion fraction, D, $D*$, and ADC of normal and cirrhotic liver parenchyma (n = 37) using 10 b values (0, 10, 20, 30, 50, 80, 100, 200, 400, and 800 sec/mm^2). They found significantly lower $D*$ and ADC in cirrhotic livers, but no difference in D and perfusion fraction between normal and cirrhotic livers. These two studies suggest that restricted diffusion observed in patients with cirrhosis reflects mostly diminished hepatic perfusion and, to a much lesser extent, pure molecular diffusion restriction. However, more data using the IVIM model correlating with dynamic contrast-enhanced MR imaging are needed to further establish advanced DW MR imaging parameters as biomarkers of fibrosis and cirrhosis.

To summarize, there is evidence of decreased capillary perfusion and/or restricted diffusion in advanced fibrosis and cirrhosis. Further studies are needed to confirm these findings and shed light on the exact mechanism of diffusion changes observed in liver fibrosis. In addition, the confounding effect of concomitant hepatic fat and/or iron deposition on ADC measurement should be examined.

Estimation of Tumor Perfusion with IVIM DW MR Imaging

As discussed above, it is possible to fractionate the calculation of the ADC if three or more b values are used at DW MR imaging. For example, if DW MR imaging is performed by using three b values of 0, 100, and 500 sec/mm^2, it would be possible to calculate the ADC by using all three b values. However, it is also possible to calculate a perfusion-insensitive ADC by using just the higher b values (100–500 sec/mm^2) or a perfusion-sensitive ADC by using the lower b values (0–100 sec/mm^2). It has been shown that it is possible to estimate perfusion fraction by comparing the ADC acquired by using only lower b values with the ADC obtained from a range that includes lower and higher b values (39,47,134). Such an approach may be relevant in a clinical trials setting, for example, for assessment of response to antiangiogenic drugs. However, in clinical practice, it is the total ADC that includes both the lower and higher b values that is most frequently used. In the research setting, it may be possible to fit a biexponential model based on the principles of IVIM when imaging is performed with multiple b values (typically more than four) (see above) (41).

Limitations of DW MR Imaging Technique in the Liver

The main limitations of DW MR imaging relate to image quality and ADC reproducibility (discussed above). Single-shot SE echo-planar DW MR imaging still has limited image quality, including poor SNR, limited spatial resolution, and echo-planar imaging–related artifacts

Radiology

(mainly distortion, ghosting, and blurring). Strategies to improve image quality are detailed in Table 3. For example, parallel imaging should be used systematically to reduce susceptibility artifacts and decrease the echo time to improve SNR (26,31,135). It is important to emphasize that DW MR imaging is an imaging technique that still often requires varying degrees of optimization to ensure consistent high-quality performance. To this end, we suggest that new clinical sites without experience with this technique should consider engaging the help of a clinical scientist, physicist, or vendor application specialists to assist in the optimization process.

Future Directions

The value of DW MR imaging for tumor detection and tumor treatment response needs to be further assessed in liver tumors treated locally or with systemic therapy, including newly developed antiangiogenic drugs.

In addition, despite the increased availability of 3.0-T imagers, there are still limited data on the use of 3.0-T DW MR imaging of the liver. High-field imaging enables higher SNR (51,52,136,137); however, echo-planar imaging results in increased susceptibility artifacts at high field. A recent study has proposed DW MR imaging as an alternative to T2-weighted imaging at 3.0 T in terms of a lower specific absorption rate (52). Non– echo-planar imaging sequences may play a role at higher field; however, data on liver DW MR imaging are still sparse (138,139).

Finally, it might be interesting to assess the value of multiparametric imaging combining DW MR imaging with other functional MR imaging techniques such as dynamic contrast-enhanced MR imaging or MR elastography for assessment of diffuse liver disease and for tumor treatment response (132,140). This should be ideally performed in a multicenter setting.

Conclusions

DW MR imaging is now available on most commercial imagers, and clinical experience with liver DW MR imaging is expanding. DW MR imaging has multiple possible applications in liver imaging, which can be summarized as follow: In the clinical setting, DW MR imaging can be used for liver lesion detection and lesion characterization, with better results compared with those of T2-weighted imaging, and with potential additional value to contrast-enhanced sequences. In the research setting, applications such as assessment of treatment response (especially in multicenter settings) and diagnosis of liver fibrosis and cirrhosis are promising; however, further confirmation is required. In addition to comparing DW MR imaging with conventional sequences, future studies should assess the value of combining DW MR imaging with conventional sequences. The radiologist has to be aware of the potential pitfalls and limitations of the technique, and we suggest that diffusion images should be interpreted in conjunction with conventional sequences. In patients who cannot receive gadolinium-based contrast agents, DW MR imaging has the potential to be a reasonable alternative technique to contrast-enhanced imaging.

References

1. Le Bihan D, Breton E, Lallemand D, Grenier P, Cabanis E, Laval-Jeantet M. MR imaging of intravoxel incoherent motions: application to diffusion and perfusion in neurologic disorders. Radiology 1986; 161:401–407.

2. Moseley ME, Cohen Y, Mintorovitch J, et al. Early detection of regional cerebral ischemia in cats: comparison of diffusion- and T2-weighted MRI and spectroscopy. Magn Reson Med 1990;14:330–346.

3. Moseley ME, Kucharczyk J, Mintorovitch J, et al. Diffusion-weighted MR imaging of acute stroke: correlation with T2-weighted and magnetic susceptibility-enhanced MR imaging in cats. AJNR Am J Neuroradiol 1990;11:423–429.

4. Moseley ME, Mintorovitch J, Cohen Y, et al. Early detection of ischemic injury: comparison of spectroscopy, diffusion-, T2-, and magnetic susceptibility-weighted MRI in cats. Acta Neurochir Suppl (Wien) 1990;51:207–209.

5. Sevick RJ, Kucharczyk J, Mintorovitch J, Moseley ME, Derugin N, Norman D. Diffusion-weighted MR imaging and T2-weighted MR imaging in acute cerebral ischaemia: comparison and correlation with histopathology. Acta Neurochir Suppl (Wien) 1990;51:210–212.

6. Warach S, Chien D, Li W, Ronthal M, Edelman RR. Fast magnetic resonance diffusion-weighted imaging of acute human stroke. Neurology 1992;42:1717–1723.

7. Schaefer PW, Grant PE, Gonzalez RG. Diffusion-weighted MR imaging of the brain. Radiology 2000;217:331–345.

8. Le Bihan D, Mangin JF, Poupon C, et al. Diffusion tensor imaging: concepts and applications. J Magn Reson Imaging 2001; 13:534–546.

9. Grobner T. Gadolinium–a specific trigger for the development of nephrogenic fibrosing dermopathy and nephrogenic systemic fibrosis? Nephrol Dial Transplant 2006; 21:1104–1108.

10. Marckmann P, Skov L, Rossen K, et al. Nephrogenic systemic fibrosis: suspected causative role of gadodiamide used for contrast-enhanced magnetic resonance imaging. J Am Soc Nephrol 2006;17:2359–2362.

11. Sadowski EA, Bennett LK, Chan MR, et al. Nephrogenic systemic fibrosis: risk factors and incidence estimation. Radiology 2007; 243:148–157.

12. Thomsen HS, Marckmann P, Logager VB. Update on nephrogenic systemic fibrosis. Magn Reson Imaging Clin N Am 2008; 16:551–560.

13. Le Bihan D. Molecular diffusion nuclear magnetic resonance imaging. Magn Reson Q 1991;7:1–30.

14. Bammer R. Basic principles of diffusion-weighted imaging. Eur J Radiol 2003;45:169–184.

15. Nicholson C, Phillips JM. Ion diffusion modified by tortuosity and volume fraction in the extracellular microenvironment of the rat cerebellum. J Physiol 1981;321:225–257.

16. Szafer A, Zhong J, Anderson AW, Gore JC. Diffusion-weighted imaging in tissues: theoretical models. NMR Biomed 1995;8:289–296.

17. Koh DM, Collins DJ. Diffusion-weighted MRI in the body: applications and challenges in oncology. AJR Am J Roentgenol 2007;188:1622–1635.

18. Stejskal EO, Tanner JE. Spin diffusion measurements: spin echoes in the presence of a time-dependent field gradient. J Chem Phys 1965;42:288–292.

19. Chenevert TL, Brunberg JA, Pipe JG. Anisotropic diffusion in human white matter: demonstration with MR techniques in vivo. Radiology 1990;177:401–405.

20. Turner R, Le Bihan D, Maier J, Vavrek R, Hedges LK, Pekar J. Echo-planar imaging of intravoxel incoherent motion. Radiology 1990;177:407–414.

21. Pierpaoli C, Jezzard P, Basser PJ, Barnett A, Di Chiro G. Diffusion tensor MR imaging of the human brain. Radiology 1996; 201:637–648.

22. Moseley ME, Cohen Y, Kucharczyk J, et al. Diffusion-weighted MR imaging of anisotropic water diffusion in cat central nervous system. Radiology 1990;176:439–445.

23. Damon BM, Ding Z, Anderson AW, Freyer AS, Gore JC. Validation of diffusion tensor MRI-based muscle fiber tracking. Magn Reson Med 2002;48:97–104.

24. Ries M, Jones RA, Basseau F, Moonen CT, Grenier N. Diffusion tensor MRI of the human kidney. J Magn Reson Imaging 2001;14:42–49.

25. Notohamiprodjo M, Glaser C, Herrmann KA, et al. Diffusion tensor imaging of the kidney with parallel imaging: initial clinical experience. Invest Radiol 2008;43:677–685.

26. Bammer R, Auer M, Keeling SL, et al. Diffusion tensor imaging using single-shot SENSE-EPI. Magn Reson Med 2002;48:128–136.

27. Bammer R, Augustin M, Strasser-Fuchs S, et al. Magnetic resonance diffusion tensor imaging for characterizing diffuse and focal white matter abnormalities in multiple sclerosis. Magn Reson Med 2000;44:583–591.

28. Chepuri NB, Yen YF, Burdette JH, Li H, Moody DM, Maldjian JA. Diffusion anisotropy in the corpus callosum. AJNR Am J Neuroradiol 2002;23:803–808.

29. Dong Q, Welsh RC, Chenevert TL, et al. Clinical applications of diffusion tensor imaging. J Magn Reson Imaging 2004;19:6–18.

30. Taber KH, Pierpaoli C, Rose SE, et al. The future for diffusion tensor imaging in neuropsychiatry. J Neuropsychiatry Clin Neurosci 2002;14:1–5.

31. Taouli B, Martin AJ, Qayyum A, et al. Parallel imaging and diffusion tensor imaging for diffusion-weighted MRI of the liver: preliminary experience in healthy volunteers. AJR Am J Roentgenol 2004;183:677–680.

32. Taouli B, Chouli M, Martin AJ, Qayyum A, Coakley FV, Vilgrain V. Chronic hepatitis: role of diffusion-weighted imaging and dif-

fusion tensor imaging for the diagnosis of liver fibrosis and inflammation. J Magn Reson Imaging 2008;28:89–95.

33. Gurses B, Kabakci N, Kovanlikaya A, et al. Diffusion tensor imaging of the normal prostate at 3 Tesla. Eur Radiol 2008;18:716–721.

34. Manenti G, Carlani M, Mancino S, et al. Diffusion tensor magnetic resonance imaging of prostate cancer. Invest Radiol 2007;42:412–419.

35. Taouli B, Vilgrain V, Dumont E, Daire JL, Fan B, Menu Y. Evaluation of liver diffusion isotropy and characterization of focal hepatic lesions with two single-shot echo-planar MR imaging sequences: prospective study in 66 patients. Radiology 2003;226:71–78.

36. Le Bihan D, Breton E, Lallemand D, Aubin ML, Vignaud J, Laval-Jeantet M. Separation of diffusion and perfusion in intravoxel incoherent motion MR imaging. Radiology 1988;168:497–505.

37. Le Bihan D. Diffusion/perfusion MR imaging of the brain: from structure to function. Radiology 1990;177:328–329.

38. Moteki T, Horikoshi H, Oya N, Aoki J, Endo K. Evaluation of hepatic lesions and hepatic parenchyma using diffusion-weighted reordered turboFLASH magnetic resonance images. J Magn Reson Imaging 2002;15:564–572.

39. Yamada I, Aung W, Himeno Y, Nakagawa T, Shibuya H. Diffusion coefficients in abdominal organs and hepatic lesions: evaluation with intravoxel incoherent motion echo-planar MR imaging. Radiology 1999;210:617–623.

40. Dixon WT. Separation of diffusion and perfusion in intravoxel incoherent motion MR imaging: a modest proposal with tremendous potential. Radiology 1988;168:566–567.

41. Luciani A, Vignaud A, Cavet M, et al. Liver cirrhosis: intravoxel incoherent motion MR imaging–pilot study. Radiology 2008;249:891–899.

42. Le Bihan D. Intravoxel incoherent motion perfusion MR imaging: a wake-up call. Radiology 2008;249:748–752.

43. Ichikawa T, Haradome H, Hachiya J, Nitatori T, Araki T. Diffusion-weighted MR imaging with a single-shot echoplanar sequence: detection and characterization of focal hepatic lesions. AJR Am J Roentgenol 1998;170:397–402.

44. Kim T, Murakami T, Takahashi S, Hori M, Tsuda K, Nakamura H. Diffusion-weighted single-shot echoplanar MR imaging for liver

disease. AJR Am J Roentgenol 1999;173:393–398.

45. Bruegel M, Holzapfel K, Gaa J, et al. Characterization of focal liver lesions by ADC measurements using a respiratory triggered diffusion-weighted single-shot echo-planar MR imaging technique. Eur Radiol 2008; 18:477–485.

46. Gourtsoyianni S, Papanikolaou N, Yarmenitis S, Maris T, Karantanas A, Gourtsoyiannis N. Respiratory gated diffusion-weighted imaging of the liver: value of apparent diffusion coefficient measurements in the differentiation between most commonly encountered benign and malignant focal liver lesions. Eur Radiol 2008;18:486–492.

47. Koh DM, Scurr E, Collins DJ, et al. Colorectal hepatic metastases: quantitative measurements using single-shot echo-planar diffusion-weighted MR imaging. Eur Radiol 2006;16:1898–1905.

48. Stehling MK, Turner R, Mansfield P. Echoplanar imaging: magnetic resonance imaging in a fraction of a second. Science 1991; 254:43–50.

49. Butts K, Riederer SJ, Ehman RL, Felmlee JP, Grimm RC. Echo-planar imaging of the liver with a standard MR imaging system. Radiology 1993;189:259–264.

50. Turner R, Le Bihan D, Chesnick AS. Echoplanar imaging of diffusion and perfusion. Magn Reson Med 1991;19:247–253.

51. Braithwaite AC, Dale BM, Boll DT, Merkle EM. Short- and midterm reproducibility of apparent diffusion coefficient measurements at 3.0-T diffusion-weighted imaging of the abdomen. Radiology 2009;250:459–465.

52. van den Bos IC, Hussain SM, Krestin GP, Wielopolski PA. Liver imaging at 3.0 T: diffusion-induced black-blood echo-planar imaging with large anatomic volumetric coverage as an alternative for specific absorption rate-intensive echo-train spin-echo sequences: feasibility study. Radiology 2008;248:264–271.

53. Chiu FY, Jao JC, Chen CY, et al. Effect of intravenous gadolinium-DTPA on diffusion-weighted magnetic resonance images for evaluation of focal hepatic lesions. J Comput Assist Tomogr 2005;29:176–180.

54. Taouli B, Sandberg A, Stemmer A, et al. Diffusion-weighted imaging of the liver: comparison of navigator triggered and breath-hold acquisitions. J Magn Reson Imaging 2009;30:561–568.

55. Koh DM, Takahara T, Imai Y, Collins DJ. Practical aspects of assessing tumors using clinical diffusion-weighted imaging in the

Radiology

body. Magn Reson Med Sci 2007;6:211–224.

56. Kwee TC, Takahara T, Ochiai R, Nievelstein RA, Luijten PR. Diffusion-weighted whole-body imaging with background body signal suppression (DWIBS): features and potential applications in oncology. Eur Radiol 2008;18:1937–1952.

57. Parikh T, Drew SJ, Lee VS, et al. Focal liver lesion detection and characterization with diffusion-weighted MR imaging: comparison with standard breath-hold T2-weighted imaging. Radiology 2008;246:812–822.

58. Nasu K, Kuroki Y, Fujii H, Minami M. Hepatic pseudo-anisotropy: a specific artifact in hepatic diffusion-weighted images obtained with respiratory triggering. MAGMA 2007;20:205–211.

59. Nasu K, Kuroki Y, Sekiguchi R, Nawano S. The effect of simultaneous use of respiratory triggering in diffusion-weighted imaging of the liver. Magn Reson Med Sci 2006;5:129–136.

60. Kwee TC, Takahara T, Koh DM, Nievelstein RA, Luijten PR. Comparison and reproducibility of ADC measurements in breathhold, respiratory triggered, and free-breathing diffusion-weighted MR imaging of the liver. J Magn Reson Imaging 2008;28:1141–1148.

61. Nasu K, Kuroki Y, Nawano S, et al. Hepatic metastases: diffusion-weighted sensitivity-encoding versus SPIO-enhanced MR Imaging. Radiology 2006;239:122–130.

62. Murtz P, Flacke S, Traber F, van den Brink JS, Gieseke J, Schild HH. Abdomen: diffusion-weighted MR imaging with pulse-triggered single-shot sequences. Radiology 2002;224:258–264.

63. de Bazelaire CM, Duhamel GD, Rofsky NM, Alsop DC. MR imaging relaxation times of abdominal and pelvic tissues measured in vivo at 3.0 T: preliminary results. Radiology 2004;230:652–659.

64. Okada Y, Ohtomo K, Kiryu S, Sasaki Y. Breath-hold T2-weighted MRI of hepatic tumors: value of echo planar imaging with diffusion-sensitizing gradient. J Comput Assist Tomogr 1998;22:364–371.

65. Hussain SM, De Becker J, Hop WC, Dwarkasing S, Wielopolski PA. Can a single-shot black-blood T2-weighted spin-echo echo-planar imaging sequence with sensitivity encoding replace the respiratory-triggered turbo spin-echo sequence for the liver? An optimization and feasibility study. J Magn Reson Imaging 2005;21:219–229.

66. Le Bihan D, Poupon C, Amadon A, Lethimonnier F. Artifacts and pitfalls in diffusion MRI. J Magn Reson Imaging 2006;24:478–488.

67. Pruessmann KP, Weiger M, Scheidegger MB, Boesiger P. SENSE: sensitivity encoding for fast MRI. Magn Reson Med 1999;42:952–962.

68. Takahara T, Imai Y, Yamashita T, Yasuda S, Nasu S, Van Cauteren M. Diffusion weighted whole body imaging with background body signal suppression (DWIBS): technical improvement using free breathing, STIR and high resolution 3D display. Radiat Med 2004;22:275–282.

69. Niendorf T, Dijkhuizen RM, Norris DG, van Lookeren Campagne M, Nicolay K. Biexponential diffusion attenuation in various states of brain tissue: implications for diffusion-weighted imaging. Magn Reson Med 1996;36:847–857.

70. Assaf Y, Cohen Y. Non-mono-exponential attenuation of water and N-acetyl aspartate signals due to diffusion in brain tissue. J Magn Reson 1998;131:69–85.

71. Gudbjartsson H, Patz S. The Rician distribution of noisy MRI data. Magn Reson Med 1995;34:910–914.

72. Sasaki M, Yamada K, Watanabe Y, et al. Variability in absolute apparent diffusion coefficient values across different platforms may be substantial: a multivendor, multiinstitutional comparison study. Radiology 2008;249:624–630.

73. Padhani AR, Liu G, Mu-Koh D, et al. Diffusion-weighted magnetic resonance imaging as a cancer biomarker: consensus and recommendations. Neoplasia 2009;11:102–125.

74. Moteki T, Sekine T. Echo planar MR imaging of the liver: comparison of images with and without motion probing gradients. J Magn Reson Imaging 2004;19:82–90.

75. Low RN, Gurney J. Diffusion-weighted MRI (DWI) in the oncology patient: value of breathhold DWI compared to unenhanced and gadolinium-enhanced MRI. J Magn Reson Imaging 2007;25:848–858.

76. Coenegrachts K, Delanote J, Ter Beek L, et al. Improved focal liver lesion detection: comparison of single-shot diffusion-weighted echoplanar and single-shot T2 weighted turbo spin echo techniques. Br J Radiol 2007;80:524–531.

77. Koh DM, Brown G, Riddell AM, et al. Detection of colorectal hepatic metastases using MnDPDP MR imaging and diffusion-weighted imaging (DWI) alone and in combination. Eur Radiol 2008;18:903–910.

78. Bruegel M, Gaa J, Waldt S, et al. Diagnosis of hepatic metastasis: comparison of respiration-triggered diffusion-weighted echo-planar MRI and five t2-weighted turbo spin-echo sequences. AJR Am J Roentgenol 2008;191:1421–1429.

79. Zech CJ, Herrmann KA, Dietrich O, Horger W, Reiser MF, Schoenberg SO. Black-blood diffusion-weighted EPI acquisition of the liver with parallel imaging: comparison with a standard T2-weighted sequence for detection of focal liver lesions. Invest Radiol 2008;43:261–266.

80. Furuhata T, Okita K, Tsuruma T, et al. Efficacy of SPIO-MR imaging in the diagnosis of liver metastases from colorectal carcinomas. Dig Surg 2003;20:321–325.

81. Vogl TJ, Schwarz W, Blume S, et al. Preoperative evaluation of malignant liver tumors: comparison of unenhanced and SPIO (Resovist)-enhanced MR imaging with biphasic CTAP and intraoperative US. Eur Radiol 2003;13:262–272.

82. Ward J, Robinson PJ, Guthrie JA, et al. Liver metastases in candidates for hepatic resection: comparison of helical CT and gadolinium- and SPIO-enhanced MR imaging. Radiology 2005;237:170–180.

83. Zech CJ, Herrmann KA, Reiser MF, Schoenberg SO. MR imaging in patients with suspected liver metastases: value of liver-specific contrast agent Gd-EOB-DTPA. Magn Reson Med Sci 2007;6:43–52.

84. Elizondo G, Fretz CJ, Stark DD, et al. Preclinical evaluation of MnDPDP: new paramagnetic hepatobiliary contrast agent for MR imaging. Radiology 1991;178:73–78.

85. Beziat C, Pilleul F, Yzebe D, Lombard-Bohas C, Mercier C, Valette PJ. Detection of liver metastases in colorectal cancer on chemotherapy. comparative study between MRI with teslascan and computed tomography with intravenous contrast media [in French]. J Radiol 2004;85:307–311.

86. Kim KW, Kim AY, Kim TK, et al. Small ($<or= 2$ cm) hepatic lesions in colorectal cancer patients: detection and characterization on mangafodipir trisodium-enhanced MRI. AJR Am J Roentgenol 2004;182:1233–1240.

87. Regge D, Campanella D, Anselmetti GC, et al. Diagnostic accuracy of portal-phase CT and MRI with mangafodipir trisodium in detecting liver metastases from colorectal carcinoma. Clin Radiol 2006;61:338–347.

88. Naganawa S, Sato C, Nakamura T, et al. Diffusion-weighted images of the liver: comparison of tumor detection before and after contrast enhancement with superparamagnetic iron oxide. J Magn Reson Imaging 2005;21:836–840.

89. Kiryu S, Watanabe M, Kabasawa H, Akahane M, Aoki S, Ohtomo K. Evaluation of super paramagnetic iron oxide-enhanced diffusion-weighted PROPELLER T2-fast spin echo magnetic resonance imaging: preliminary experience. J Comput Assist Tomogr 2006;30:197–200.

90. Coenegrachts K, Matos C, Ter Beek L, et al. Focal liver lesion detection and characterization: comparison of non-contrast enhanced and SPIO-enhanced diffusion-weighted single-shot spin echo echo planar and turbo spin echo T2-weighted imaging. Eur J Radiol 2008; Epub ahead of print.

91. Inan N, Arslan A, Akansel G, et al. Diffusion-weighted imaging in the differential diagnosis of simple and hydatid cysts of the liver. AJR Am J Roentgenol 2007; 189:1031–1036.

92. Muller MF, Prasad P, Siewert B, Nissenbaum MA, Raptopoulos V, Edelman RR. Abdominal diffusion mapping with use of a whole-body echo-planar system. Radiology 1994;190:475–478.

93. Demir OI, Obuz F, Sagol O, Dicle O. Contribution of diffusion-weighted MRI to the differential diagnosis of hepatic masses. Diagn Interv Radiol 2007;13:81–86.

94. Vossen JA, Buijs M, Liapi E, Eng J, Bluemke DA, Kamel IR. Receiver operating characteristic analysis of diffusion-weighted magnetic resonance imaging in differentiating hepatic hemangioma from other hypervascular liver lesions. J Comput Assist Tomogr 2008;32:750–756.

95. Goshima S, Kanematsu M, Kondo H, et al. Hepatic hemangioma: correlation of enhancement types with diffusion-weighted MR findings and apparent diffusion coefficients. Eur J Radiol 2009;70:325–330.

96. Moteki T, Ishizaka H, Horikoshi H, Matsumoto M. Differentiation between hemangiomas and hepatocellular carcinomas with the apparent diffusion coefficient calculated from turboFLASH MR images. J Magn Reson Imaging 1995;5:187–191.

97. Chan JH, Tsui EY, Luk SH, et al. Diffusion-weighted MR imaging of the liver: distinguishing hepatic abscess from cystic or necrotic tumor. Abdom Imaging 2001;26:161–165.

98. Goshima S, Kanematsu M, Kondo H, et al. Diffusion-weighted imaging of the liver: optimizing b value for the detection and characterization of benign and malignant hepatic lesions. J Magn Reson Imaging 2008;28:691–697.

99. Koinuma M, Ohashi I, Hanafusa K, Shibuya H. Apparent diffusion coefficient measurements with diffusion-weighted magnetic resonance imaging for evaluation of hepatic fibrosis. J Magn Reson Imaging 2005;22:80–85.

100. Hamstra DA, Rehemtulla A, Ross BD. Diffusion magnetic resonance imaging: a biomarker for treatment response in oncology. J Clin Oncol 2007;25:4104–4109.

101. Sharma U, Danishad KK, Seenu V, Jagannathan NR. Longitudinal study of the assessment by MRI and diffusion-weighted imaging of tumor response in patients with locally advanced breast cancer undergoing neoadjuvant chemotherapy. NMR Biomed 2009;22:104–113.

102. Thoeny HC, De Keyzer F, Vandecaveye V, et al. Effect of vascular targeting agent in rat tumor model: dynamic contrast-enhanced versus diffusion-weighted MR imaging. Radiology 2005;237:492–499.

103. Mardor Y, Roth Y, Ochershvilli A, et al. Pretreatment prediction of brain tumors' response to radiation therapy using high b-value diffusion-weighted MRI. Neoplasia 2004;6:136–142.

104. Patterson DM, Padhani AR, Collins DJ. Technology insight: water diffusion MRI–a potential new biomarker of response to cancer therapy. Nat Clin Pract Oncol 2008;5:220–233.

105. Geschwind JF, Artemov D, Abraham S, et al. Chemoembolization of liver tumor in a rabbit model: assessment of tumor cell death with diffusion-weighted MR imaging and histologic analysis. J Vasc Interv Radiol 2000;11:1245–1255.

106. Deng J, Rhee TK, Sato KT, et al. In vivo diffusion-weighted imaging of liver tumor necrosis in the VX2 rabbit model at 1.5 Tesla. Invest Radiol 2006;41:410–414.

107. Yuan YH, Xiao EH, Liu JB, et al. Characteristics of liver on magnetic resonance diffusion-weighted imaging: dynamic and image pathological investigation in rabbit liver VX-2 tumor model. World J Gastroenterol 2008;14:3997–4004.

108. Youn BJ, Chung JW, Son KR, et al. Diffusion-weighted MR: therapeutic evaluation after chemoembolization of VX-2 carcinoma implanted in rabbit liver. Acad Radiol 2008;15:593–600.

109. Deng J, Virmani S, Young J, et al. Diffusion-weighted PROPELLER MRI for quantitative assessment of liver tumor necrotic fraction and viable tumor volume in VX2 rabbits. J Magn Reson Imaging 2008;27:1069–1076.

110. Ohira T, Okuma T, Matsuoka T, et al. FDG-MicroPET and diffusion-weighted MR image evaluation of early changes after radiofrequency ablation in implanted VX2 tumors in rabbits. Cardiovasc Intervent Radiol 2009; 32:114–120.

111. Yuan YH, Xiao EH, Liu JB, et al. Characteristics and pathological mechanism on magnetic resonance diffusion-weighted imaging after chemoembolization in rabbit liver VX-2 tumor model. World J Gastroenterol 2007;13:5699–5706.

112. Koh DM, Scurr E, Collins D, et al. Predicting response of colorectal hepatic metastasis: value of pretreatment apparent diffusion coefficients. AJR Am J Roentgenol 2007;188:1001–1008.

113. Cui Y, Zhang XP, Sun YS, Tang L, Shen L. Apparent diffusion coefficient: potential imaging biomarker for prediction and early detection of response to chemotherapy in hepatic metastases. Radiology 2008;248:894–900.

114. Buijs M, Vossen JA, Hong K, Georgiades CS, Geschwind JF, Kamel IR. Chemoembolization of hepatic metastases from ocular melanoma: assessment of response with contrast-enhanced and diffusion-weighted MRI. AJR Am J Roentgenol 2008;191:285–289.

115. De Santis M, Torricelli P, Cristani A, et al. MRI of hepatocellular carcinoma before and after transcatheter chemoembolization. J Comput Assist Tomogr 1993;17:901–908.

116. De Santis M, Alborino S, Tartoni PL, Torricelli P, Casolo A, Romagnoli R. Effects of lipiodol retention on MRI signal intensity from hepatocellular carcinoma and surrounding liver treated by chemoembolization. Eur Radiol 1997;7:10–16.

117. Kamel IR, Bluemke DA, Ramsey D, et al. Role of diffusion-weighted imaging in estimating tumor necrosis after chemoembolization of hepatocellular carcinoma. AJR Am J Roentgenol 2003;181:708–710.

118. Kamel IR, Bluemke DA, Eng J, et al. The role of functional MR imaging in the assessment of tumor response after chemoembolization in patients with hepatocellular carcinoma. J Vasc Interv Radiol 2006;17:505–512.

119. Chen CY, Li CW, Kuo YT, et al. Early response of hepatocellular carcinoma to transcatheter arterial chemoembolization: choline levels and MR diffusion constants–initial experience. Radiology 2006;239:448–456.

120. Deng J, Miller FH, Rhee TK, et al. Diffusion-weighted MR imaging for determination of hepatocellular carcinoma response to yttrium-90 radioembolization. J Vasc Interv Radiol 2006;17:1195–1200.

121. Kamel IR, Reyes DK, Liapi E, Bluemke DA, Geschwind JF. Functional MR imaging assessment of tumor response after 90Y

microsphere treatment in patients with unresectable hepatocellular carcinoma. J Vasc Interv Radiol 2007;18:49–56.

122. Kamel IR, Liapi E, Reyes DK, Zahurak M, Bluemke DA, Geschwind JF. Unresectable hepatocellular carcinoma: serial early vascular and cellular changes after transarterial chemoembolization as detected with MR imaging. Radiology 2009;250:466–473.

123. Mannelli L, Kim S, Hajdu C, Babb J, Clark TW, Taouli B. Assessment of tumor necrosis of hepatocellular carcinoma after chemoembolization: diffusion-weighted and contrast-enhanced MRI with histopathologic correlation of the explanted liver. AJR Am J Roentgenol 2009;193:1044–1052.

124. Goshima S, Kanematsu M, Kondo H, et al. Evaluating local hepatocellular carcinoma recurrence post-transcatheter arterial chemoembolization: Is diffusion-weighted MRI reliable as an indicator? J Magn Reson Imaging 2008;27:834–839.

125. Namimoto T, Yamashita Y, Sumi S, Tang Y, Takahashi M. Focal liver masses: characterization with diffusion-weighted echo-planar MR imaging. Radiology 1997;204:739–744.

126. Amano Y, Kumazaki T, Ishihara M. Single-shot diffusion-weighted echo-planar imaging of normal and cirrhotic livers using a phased-array multicoil. Acta Radiol 1998;39:440–442.

127. Aubé C, Racineux PX, Lebigot J, et al. Diagnosis and quantification of hepatic fibro-

sis with diffusion weighted MR imaging: preliminary results [in French]. J Radiol 2004;85:301–306.

128. Lewin M, Poujol-Robert A, Boelle PY, et al. Diffusion-weighted magnetic resonance imaging for the assessment of fibrosis in chronic hepatitis C. Hepatology 2007; 46:658–665.

129. Girometti R, Furlan A, Esposito G, et al. Relevance of b-values in evaluating liver fibrosis: a study in healthy and cirrhotic subjects using two single-shot spin-echo echoplanar diffusion-weighted sequences. J Magn Reson Imaging 2008;28:411–419.

130. Taouli B, Tolia AJ, Losada M, et al. Diffusion-weighted MRI for quantification of liver fibrosis: preliminary experience. AJR Am J Roentgenol 2007;189:799–806.

131. Annet L, Materne R, Danse E, Jamart J, Horsmans Y, Van Beers BE. Hepatic flow parameters measured with MR imaging and Doppler US: correlations with degree of cirrhosis and portal hypertension. Radiology 2003;229:409–414.

132. Hagiwara M, Rusinek H, Lee VS, et al. Advanced liver fibrosis: diagnosis with 3D whole-liver perfusion MR imaging–initial experience. Radiology 2008;246:926–934.

133. Annet L, Peeters F, Abarca-Quinones J, Leclercq I, Moulin P, Van Beers BE. Assessment of diffusion-weighted MR imaging in liver fibrosis. J Magn Reson Imaging 2007; 25:122–128.

134. Coenegrachts K, Delanote J, Ter Beek L, et al. Evaluation of true diffusion, perfusion factor, and apparent diffusion coefficient in non-necrotic liver metastases and uncomplicated liver hemangiomas using black-blood echo planar imaging. Eur J Radiol 2009;69:131–138.

135. Bammer R, Keeling SL, Augustin M, et al. Improved diffusion-weighted single-shot echoplanar imaging (EPI) in stroke using sensitivity encoding (SENSE). Magn Reson Med 2001;46:548–554.

136. Lee VS, Hecht EM, Taouli B, Chen Q, Prince K, Oesingmann N. Body and cardiovascular MR imaging at 3.0 T. Radiology 2007;244:692–705.

137. Barth MM, Smith MP, Pedrosa I, Lenkinski RE, Rofsky NM. Body MR imaging at 3.0 T: understanding the opportunities and challenges. RadioGraphics 2007;27:1445–1462; discussion 1462–1464.

138. Deng J, Miller FH, Salem R, Omary RA, Larson AC. Multishot diffusion-weighted PROPELLER magnetic resonance imaging of the abdomen. Invest Radiol 2006;41:769–775.

139. Deng J, Omary RA, Larson AC. Multishot diffusion-weighted SPLICE PROPELLER MRI of the abdomen. Magn Reson Med 2008; 59:947–953.

140. Talwalkar JA. Elastography for detecting hepatic fibrosis: options and considerations. Gastroenterology 2008;135:299–302.